

# Neural Control of Redundant (Abundant) Systems as Algorithms Stabilizing Subspaces

V. M. Akulin<sup>1,2,3</sup>, and F. Carrier<sup>1</sup>  
and

Stanislaw Solnik<sup>4,5</sup>, and M.L. Latash<sup>4,6</sup>

<sup>1</sup>Laboratoire Aimé Cotton, CNRS II, Bâtiment 505, 91405 Orsay  
Cedex, France

<sup>2</sup>Laboratoire Jean-Victor Poncelet, CNRS, 11 Bolshoy Vlasyevskiy Pereulok,  
Moscow, 119002, Russia

<sup>3</sup>Institute for Information Transmission Problems of the Russian Academy of Science,  
Bolshoy Karetny per. 19, Moscow, 127994, Russia

<sup>4</sup>Pennsylvania State University, University Park PA 16802, USA

<sup>5</sup>University School of Physical Education, Wroclaw, Poland

<sup>6</sup>Moscow Institute of Physics and Technology, 9 Institutskiy per., Dolgoprudny,  
Moscow Region, 141700, Russia

the date of receipt and acceptance should be inserted later

**Abstract** We address the problem of stability of motor actions implemented by the central nervous system based on simple algorithms potentially reflecting physical (including physiological) processes within the body. A number of conceptually simple algorithms that solve motor tasks with a high probability of success may be based on feedback schemes that ensure stability of subspaces of neural variables associated with accomplishing those tasks. The task is formulated in terms of linear constraints imposed either on the human body mechanical variables or on neural variables; we discuss three reference frames relevant to these processes. We discuss underlying basic principles of such algorithms, their architecture, and efficiency, and compare the outcomes of implementation of such algorithms with the results of experiments performed on the human hand.

## Contents

1	Introduction: The Nervous System, Motor Control, and Stability Search Problem . . . . .	1
2	The Stability Search Algorithms, Dynamics Control, and the Effect of Noise . . . . .	3
3	Experiments with Human Hand . . . . .	13
4	Discussion: The Stability Search Algorithm Hypotheses within the Context of Motor Control Hypotheses . . . . .	18

Address(es) of author(s) should be given

## 1 Introduction: The Nervous System, Motor Control, and Stability Search Problem

Many functions of the central nervous system (CNS) can be described as combining numerous elements (we will refer to their outputs as elemental variables) into relatively low-dimensional sets related to such functions as cognition, perception, and action. The existence of such low-dimensional sets ensures stability of percepts, thoughts, and actions despite the variable contributions from the elements (sensory receptors, neurons, motor units, etc.) and changes in the environment. Here, we try to offer a mathematical description of processes that could bring about such stability based on variability. The aim of this paper is not to mimic a control algorithm for some particular task, which the CNS solves, but rather to find a conceptual framework, though vague at the moment, which would allow one to offer mathematical principles that can shape neural activity associated with a variety of tasks. We use, as an example, the production of voluntary movements by redundant sets of elements. Our approach is not based on an a priori cost function, but on an intuitive, simple algorithmic principle. Of course, starting from a very complex algorithm may have an a priori advantage in achieving high probability of success as compared to simpler algorithms. We start building a model from a linear dynamic system and then add operational complexity as

needed to achieve a reasonable success probability. At any level of description, the system for movement production is apparently redundant [4]. This means that the number of its elemental state variables is larger than the number of constraints associated with typical tasks. Depending on the selected level of analysis, elements and elemental variables are defined differently (reviewed in [18]). For example, kinematic analysis of multi-joint action frequently considers individual joint rotations as elemental variables. Kinetic analysis of the force and moment production by parallel chains (such as the digits of the human hand) may consider forces/moments produced by the digits as elemental variables. Analysis of muscle activation may be based on firing patterns of individual motor units as elemental variables. And so on. The apparent redundancy typical of all these examples has been re-cast as abundance [11, 17] to emphasize that the extra elemental variables are not the sources of computational problems for the CNS but an essential component of the design that allows combining stability of actions with flexibility of performance (changing actions, responding to perturbations, performing several actions in parallel, etc.).

Consider the following example as an illustrations of our goal and approach. Imagine a walking person who suddenly steps on a slippery surface. The slip is typically followed by a very complex pattern of movements of all body parts resulting in restoring balance in a large percentage of cases. Each time a slip occurs the movement pattern looks unique. We assume here that such highly variable patterns emerge as a result of a single, relatively simple algorithm applied to cases with varying initial conditions at the slip. What could be the search algorithm for new stability, presumably formulated as a set of simple rules realized by the physical/physiological system without explicit computational steps? What is the success rate of not falling yielded by such an algorithm? We expect a balance between the operational simplicity of the algorithm and the success probability. What could be the relation of such an algorithm to established notions in the field of motor control such as hierarchical control and uncontrolled manifold hypothesis[27]?

In the most simple mathematical setting, the equilibrium control problem (task) can be seen as a linear requirement  $Y_j = \sum_{i=1}^N \alpha_{j,i} x_i$  imposed to  $N$  elemental variables  $x_i$  (with  $i$  running from 1 to  $N$ ) describing states of a redundant set of effectors, which depends on desired position of the object given by a set of variables  $Y_j$  (with  $j$  running from 1 to  $M$ ). The task is to make the subspace determined by this set of linear conditions mechanically stable, that is to find a proper feedback

matrix  $\beta_{i,j}$ , which via the equation

$$\dot{x}_i = \sum_{j=1}^M \beta_{i,j} (y_j - Y_j) \quad (1)$$

relates the time derivatives  $\dot{x}_i$  of the elemental variables and the deviations  $\delta y_j = y_j - Y_j$  of instantaneous coordinates  $y_i$  of the controlled object from their desired positions  $Y_j$ . One has to construct a simple algorithm of yielding such a feedback matrix  $\beta_{i,j}$  for an arbitrarily predetermined task matrix  $\alpha_{j,i}$ .

If now one eliminates the physical aspect of the problem and treats the variables  $x_i$  and  $y_j$  as certain brain variables responsible for the control of a physical object, then the model begins to describe a purely mental process that operates with some neural variables  $x_i$  responsible for the effector activity and the neural variables  $y_j$  responsible for the perception of the controlled object state, whereas the matrix  $\alpha_{j,i}$  connects these two groups of variables. Here, we suggest a sequence of general principles that may be seen as extensions of the idea that biological systems are reasonably sloppy [15,20]. Under this expression, we mean that approximate solutions may be generated for typical tasks as long as they lead to success with acceptable probability. This notion is closely related to the notion of satisficing coined by Herbert Simon [29]. This means that they do not solve problems exactly but rather use simplified rules that produce solutions that are good enough (e.g., successful most of the time). From the mathematical point of view, even for a simple linear model, construction of a feedback algorithm is a nonlinear process, which is meant to vary the matrix elements of  $\beta_{i,j}$  depending on the size and the evolution history of variables  $x_i$ . First, we suggest a requirement, that the algorithm should rely, as much as possible, on local actions, that is, on actions that change the way a neural variable  $x_i$  participates in the feedback, such that the decision to undertake an action is based on the actual and previous values  $x_i(t < t_{actual})$  of this very variable, whereas other variable do not affect the decision. However, such a purely local algorithm may be incapable of providing good stability properties, and thus one needs to involve non-local actions, when the participation of one variable depends on the state and the evolution history of other variables. In such a case, our second principle is that the number of nonlocal interventions should be kept at a minimum. Third, we would like to formulate the decision criteria in simple, intuitive terms. In this study, we start with a rule "Act on the most nimble" (the AMN-rule), when changes in the local parameters occur for the most unstable variable first.

Two more points should be discussed in the context of the requirements imposed on the algorithm. (i) It is desirable that the algorithm ensures robustness of the feedback and yields such  $\beta_{i,j}$  that can be used across the task  $\alpha_{j,i}$  within certain limits. Formally this implies that the spectrum  $\{\omega_m\}$  of eigenvalues of the matrix  $\omega_{jj'} = \sum_{i=1}^N \alpha_{j,i} \beta_{i,j'}$  remains stable (with negative real parts) even when the task matrix experiences a perturbation  $\delta\alpha_{j,i}$ . (ii) It is hard to imagine a direct experimental access to the assumed neural variables. Since the classical works by the group of Georgopoulos [30,31], studies of cortical neuronal population vectors have provided plenty of evidence that such vectors correlate with kinematic movement characteristics [32,33]. We would like to emphasize, however, that such correlations are strongly dependent on the external conditions of the experiments and do not prove the physical meaning of the population vectors. In contrast, we are implying neural variables directly related to parameters related to setting a task in a multi-dimensional space of elemental variables and participating in stabilization of its performance. Fortunately, analysis of the mathematical structure of the problem can rely on the noise statistics. The reason for this is the fact that, for a rather general model of noise, one can find a Gaussian distribution of the measurements in the  $M$ -dimensional space of the observed variables  $y_j$ , while the eigenvectors of the covariance matrix of this distribution coincides with the eigenvectors of  $\omega_{jj'}$ , and a certain relation among the eigenvalues can be deduced.

The "act on the most nimble" rule makes our model essentially non-linear. However, in-between successive actions on the most nimble variables, the dynamical system can be treated as linear and open, which implies its being subjected to noise, defined as uncontrollable small and random deviations of the coordinates from their averages over short time intervals. Though biological systems typically do not manifest Gaussian noise statistics, the basic characteristics, such as noise covariance matrix, still can reveal important instantaneous characteristics of the matrix governing the linear part of dynamics, such as eigenvectors and, to a certain extent, eigenvalues, thus helping to compare calculated and observed results.

## 2 The Stability Search Algorithms, Dynamics Control, and the Effect of Noise

In this Section we discuss the main ideas underlying construction of the stability search algorithms. We start by discussing the mathematical complexity of the problem, and specific requirements for solving this problem by an analog computer - a model for the CNS at this

stage. In this context we talk about local algorithms contrasting them to the non-local ones and introduce a new basis of neural variables where such local algorithms can be implemented.

We continue by exploring the ingredients required for the stabilization algorithm construction. By proposing a simple model of the control we specify the problem in terms of a task and a feedback matrices, showing that a random choice of the feedback has extremely low chances of yielding the required stabilization. We next turn to the simplest local equilibrium search algorithm - "act on the most nimble", which can considerably increase the chances of stabilization gaining. This idea turns to be even more efficient when the feedback matrix is not random, but is tailored in a way which we call "generations" structure, - where each one-dimensional subspace is coupled to a multidimensional "generation" of variables, that all have typical velocities ("nimbleness") of the same order of magnitude. Each "generation" has "nimbleness" considerably slower that for the previous one and much higher than for the next "generation". This idea is further developed when we account for the possibility of non-local actions, where each next generation, when started at a relevant time scale to implement local operations, is also allowed to inhibits activity of previous generations. This is followed by analysis of the case where each generation nimbleness is a tunable fit parameter, and a solution can always be found, for a system of any dimensionality, although this solution rely on the typical velocities that may differ by many orders of magnitude for the first and the last generations.

The next topic we discuss in this Section is the relations between noise and stability, which later on will help us to gain a deeper insight into the dynamics of the system by analyzing experimentally observed covariances of the noise. The term "noise" is ambiguous in neurophysiology (reviewed in [35]). For example, during quiet standing, humans show spontaneous deviations of the body from the vertical (postural sway), which are a superposition of two components, rambling and trembling [43]. The former reflects migration of the equilibrium point with respect to which balance is organized, while the latter reflects oscillations about that moving equilibrium point. Rambling has been viewed as a reflection of an unintentional but meaningful search for limits of stability and, hence, it would be counterintuitive to classify it as "noise". Nevertheless, for the purposes of the current study, we will use "noise" to imply spontaneous variance in physiological signals that is not related to the explicit task and is not induced by an identifiable external perturbation. We understand

that this definition may attribute to noise physiologically meaningful processes.

We conclude the Section by considering a realistic realization of the control algorithm in hierarchical systems, show that for this architecture of the feedback damping of the dynamic variables is indispensable and propose a model of self-adjusting damping, which yields time dependencies of the dynamic variables resembling ones observed experimentally.

## 2.1 Control Complexity and Coordinate Frames

Finding solution of  $M$  linear equations  $Y_j = \sum_{i=1}^N \alpha_{j,i} x_i$  for  $N > M$  variables is a problem of a polynomial complexity  $\sim M^2$ . It is sufficient to take the first  $M$  columns of the  $M \times N$  matrix  $\alpha_{i,j}$  and invert the resulting  $M \times M$  square matrix, provided it is not degenerate. Solutions of the problem for the first  $M$  variables  $\{x_1 \dots x_M\}$  form a  $M$ -dimensional subspace  $S_M$  in the entire  $N$ -dimensional space, parametrized by the remaining  $N - M$  variables  $\{x_{M+1} \dots x_N\}$ . Construction of the inverse matrix  $\alpha_{i,j}^{-1}$  based on the sequential finding of its line vectors complemented by the orthonormalization of these vectors with those found earlier indeed implies the number of operations on the order of  $M^2$ .

To solve this problem on an analog computer, one should construct and implement a dynamic process that has the  $M$ -dimensional subspace  $S_M$  as a stable stationary manifold, as suggested by Eq.(1). Apparently, the additional requirement of stability augments the mathematical complexity of the relevant algorithm, but once this requirement is fulfilled, the result offers an advantageous generalization – it can be implemented for solving systems of nonlinear equations that is a problem of a much higher complexity. Here, we are going to propose several strategies of constructing heuristic algorithms that result in the dynamic stabilization of subspaces defined by systems of  $M$  equations for  $N > M$  variables.

Two points have to be elucidated. The first is that, according to the general vision, an analog computer is a collection of rather simple, although linearly interacting, dynamic systems - elements, while the algorithms are viewed in this context as sequences of instrumental prescriptions of how to modify these interactions. Each of the prescribed conditions is imposed on the value of a dynamic variable describing the state of one element and the prescribed action is applied to the same or to another element. Prescribed action on one chosen element that depends only on the state of either that element or on another chosen element implies so-called locality or bi-locality, respectively, of the elementary

step of the algorithms. The second point is that non-linearity of the analog computer generated by such a local and/or bi-local algorithm may not result in universal stability of the dynamics. In other words, for some initial conditions the system may reach a stationary solution, while for other initial conditions it becomes unstable. In such a situation, one can speak about the success rate  $R(N, M)$  of the algorithm, and this statistical quantity serves as its quality characteristic.

We now move to implementing the two principles mentioned in the Introduction: (1) Reliance primarily on local actions while nonlocal actions are minimally involved; and (2) Using the intuitive AMN-rule. First, we introduce three types of specific bases related to certain linear combinations of the body variables. First, there is a *measurement* basis formed by experimentally accessible variables, for example positions, forces, or muscle activations. Second, there is another, task-dependent, basis formed by so-called *modes*, that are linear combinations of the former variables independently fluctuating under the action of noise and coinciding with the eigenvectors of the aforesaid matrix  $\omega_{j,j'}$  (cf. [6,14]). The modes are expected to be stable for broad ranges of tasks and not to change without specialized training. The third basis is the reference system relying on the variables  $x_i$  responsible for the control over the body state. To our knowledge, this coordinate system has not been defined previously. Each of the coordinates of the third system represents combinations of modes that are task specific and relatively quickly adjustable to changes in the external conditions of task execution, for example to changes in stability requirements (e.g. [3]). This basis comprises the variables that experience local control, that is, changes in the feedback loop gain with respect to each of these variables  $x_i$  produced once a certain functional  $z_i \{x_i(t)\}$  of these very variable reaches a critical value. Such gain changes may occur gradually with changes in the value of the functional. To summarize, the task is considered within a preexisting, task-dependent basis.

## 2.2 The Control Structure

To solve the problem of a subspace stabilization one first takes an arbitrarily  $M \times N$  matrix  $\hat{\alpha}$  that imposes conditions of Eq.(1) with  $Y_i = 0$  thus defining the required subspace  $S_M = \{y_i = 0\}$ . Thus the task is to find a  $N \times M$  linear feedback matrix  $\hat{\beta}$  that, by determining the derivatives

$$\frac{d}{dt} x_i = \sum_{j=1}^M \beta_{i,j} y_j, \quad (2)$$

prescribes the modifications of  $\{x_i\}$  leading towards the subspace  $S_M$ . Dynamics of the system is therefore given by the equation

$$\frac{d}{dt}x_i = \sum_{j=1}^N \sum_{k=1}^M \beta_{i,k} \alpha_{k,j} x_j. \quad (3)$$

and a stable  $M$ -dimensional subspace  $S_M$  exists in the  $N$ -dimensional space if all the non-zero eigenvalues of the degenerate square  $N \times N$  matrix  $\widehat{\Omega} = \widehat{\beta}\widehat{\alpha}$  of the rank  $M$  have negative real parts. The probability to satisfy this requirement for randomly chosen either  $\widehat{\alpha}$  or both  $\widehat{\alpha}$  and  $\widehat{\beta}$  is rather low, and in order to stabilize  $S_M$  with a high enough success rate  $R(N, M)$  for a chosen  $\widehat{\alpha}$ , a randomly or systematically chosen linear feedback matrix  $\widehat{\beta}_{\text{initial}}$  may need to be modified  $\widehat{\beta}_{\text{initial}} \rightarrow \widehat{\beta}_{\text{modified}}$  once it does not ensure negativity of the  $\widehat{\beta}\widehat{\alpha}$  eigenvalues real parts and hence does not yield the required stabilization. A sequence of the modifications  $\widehat{\beta}_{\text{modified}(n)} \rightarrow \widehat{\beta}_{\text{modified}(n+1)}$  can be continued according to a certain algorithm until stabilization is achieved.

Each elementary act of the modification algorithm rely on three main ingredients: (i) the variable  $x_i$  initiating the action, (ii) type of the action itself  $\widehat{\beta}_{\text{modified}(n)} = \widehat{\mathbf{G}}\widehat{\beta}_{\text{modified}(n+1)}$  implementing the modification  $\widehat{\beta}_{\text{modified}(n)} \rightarrow \widehat{\beta}_{\text{modified}(n+1)}$ , which is specified by a non-linear functional matrix  $\widehat{\mathbf{G}}(\{x_f(t)\}, \{x_i(t)\})$ , and (iii) the variable  $x_f$  subject to the action. Once the source and the target variables coincide, we encounter a so-called local algorithm, which implies that for  $f \neq i$  we deal with a non-local elementary act of the algorithm. During last decades, the difference between local and non-local actions are has been widely discussed in the context of Quantum Informatics, where physical implementation of non-local transformations, so-called quantum gates, is a much more challenging experimental task as compared to local transformations. In a situation where each variable  $x_k$  is associated with some location in space, the situation typical of Quantum Informatics becomes generic: Local algorithms are much easier to implement in a physical realization of the controlled systems than non-local ones since they do not require transportation of the nonlinear action from one spatial location to another.

### 2.2.1 No algorithm

We first consider the simplest realization of an analog computer working without a controlling algorithm. For the sake of presentation simplicity, assume that the desired subspace  $S_M$  corresponds to zero values of all the variables  $y_{i \in \{1, M\}}$ . Non-zero values of these variables

will thus be employed as entries into the feedback loop given by a rectangular  $N \times M$  matrix  $\beta_{i,j}$ , such that Eq.(2) holds, while Eq.(3) describes the system dynamics.

For a generic rectangular randomly chosen matrix  $\alpha_{i,j}$  and the randomly chosen feedback matrix  $\beta_{i,k}$  the success rate  $R(N, M)$  found numerically scales approximately as  $2^{-M}$ , which is consistent with the assumption that all non-zero eigenvalues of the matrix  $\widehat{\Omega}$  may have the real parts both negative and positive with equal probability and, roughly speaking, different eigenvalues are statistically independent one from one another.

### 2.2.2 Local algorithm for random feedback

Our aim now is to construct a control algorithm, which is capable of improving the success rate. We call this algorithm the AMN-rule later. We begin with the simplest case of a local algorithm by assuming that the feedback sign for a given  $x_i$  changes once a positive quantity

$$z_i(t) = \int_0^t \left( \frac{dx_i}{dt} \right)^2 dt \quad (4)$$

exceeds a threshold value  $Z$ . This represent an example of "act on the most nimble" control, where, as a first guess, we consider the integral of the rates squared, which is an analog of the strictly positive dissipated heat functional typical of electrical circuits. Further, we will consider other strictly positive functionals. Formally, the local control implies that the set of equations (3) is modified by the presence of a sign function and reads

$$\frac{d}{dt}x_i = G_{ii} \sum_{j=1}^N \sum_{k=1}^M \beta_{i,k} \alpha_{k,j} x_j \quad (5)$$

$$G_{ii} = \text{sign}(Z - z_i(t)). \quad (6)$$

This strategy yields 100% success rate for the case of  $M = 1$ , that is the case where the matrix  $\widehat{\beta}\widehat{\alpha}$  has rank 1. In this case the dynamic process occurs in a subspace of the dimension 1 such that the dynamic equation

$$\frac{d}{dt}y_1 = \sum_{i=1}^N \alpha_{1,i} G_{ii} \beta_{i,1} y_1 \quad (7)$$

for the variable  $y_1 = \sum_{i=1}^N \alpha_{1,i} x_i$  determines time dependencies of all the other variables  $x_i = \beta_{i,1} y_1$ . Indeed, if the quantity  $\omega = \sum_{i=1}^N \alpha_{1,i} \beta_{i,1}$  is positive,  $y_1$  exponentially increases in time. This means that the variable  $x_i$  corresponding to the largest  $|\beta_{i,1}|$  produces the highest "Joule's heat"  $z_i(t)$  and at some moment of time, when this quantity exceeds the threshold value

$M$	1	2	3	4	4	4	5
$N$	10	20	30	15	40	60	30
$R_{\text{random}}$	0.50	0.24	0.14	—	0.06	—	—
$R_{\text{local}}$	1	0.77	0.46	0.17	0.16	0.154	0.06
$R_{\text{tailored}}$	1	0.85	0.62	0.32/0.28	0.36	0.31	0.25/0.21
$R_{\text{generations}}$	1	0.9	0.68	0.42/0.46	0.66	—	0.45/0.31

**Table 1** The success rate of various algorithms stabilizing  $M$ -dimensional subspace of  $N$ -dimensional space.

$Z$ , the sign of  $\text{sign}(Z - z_i(t))\beta_{i,1}$  changes. For a positive  $\alpha_{1,i}$ , this results in a decrease of  $\omega$  and slowing-down of the instability. For a random matrix  $\hat{\alpha}$ , however, the matrix element  $\alpha_{1,i}$  can equally be negative or positive; in the latter case, the change of the sign results in the instability speeding-up. In this case, the exponential growth of the variables  $x_i$  continues, and after awhile, the next biggest  $|\beta_{i,1}|$  leads to a change of the corresponding feedback sign. Changes of the signs continue till  $\omega$  becomes negative, and the dynamic process becomes stable. This will definitely occur for the matrix  $\hat{\beta}$  of the rank 1, but for higher ranks this stabilization may not happen. Moreover, numerical search shows that the success rate  $R_{\text{local}}$  of such stabilization drops with the increasing rank  $M$ . The results of the numerical simulation for this case are shown in Table 1, the fourth row ( $R_{\text{local}}$ ). These results have to be compared with  $R_{\text{random}}$  for the not controlled random feedback. While the success rate is higher for the controlled system for all  $M$  and  $N$ , it drops rather quickly with the rank  $M$ , while being relatively less sensitive to  $N$  (compare the  $R$  values for  $M = 4$  and  $N = 15, 40$ , and  $60$ ).

### 2.2.3 Tailored linear feedback and the local algorithm

Remaining within the general case of Eq. (5), we replace the random feedback matrix  $\beta_{i,j}$  by another one, constructed to augment the success rate for higher  $M$ . We take it in the form

$$\hat{\beta} = \begin{pmatrix} \vec{v} & 0 & 0 & \dots & 0 \\ 0 & q\vec{v} & 0 & \dots & 0 \\ 0 & 0 & q^2\vec{v} & \dots & 0 \\ \dots & \dots & \dots & \dots & \dots \\ 0 & 0 & 0 & \dots & q^{M-1}\vec{v} \end{pmatrix} \quad (8)$$

where  $\vec{v}$  is a column vector of the size of the ratio  $N/M$ , which we assume to be an integer. Here  $q$  is a small parameter, which ensures that at each time scale  $\sim q^{-n}$ , one has to deal with a subspace of rank just 1 with the same algorithm as for the case of  $M = 1$ , while the subspaces corresponding to the larger matrix elements  $\sim q^{-k < n}$  are assumed to have already been stabilized earlier.

In simple words the main idea is: there are generations of elemental variables organized by their expected nimbleness, which scales as  $q^g$ , that is, exponentially with the number  $g$  of the generation. The controller uses the AMN-rule within an appropriate channel (which is a set of variables  $x_i$  grouped by their common input from a component of the vector  $\vec{y}$ ) and then deals with the next most nimble channel without returning to the first one, and so on. This approach improves the success rate for higher  $M$ ; however, even it cannot guarantee 100% convergence. The results of the numerical work for the success rate  $R_{\text{tailored}}$  in the case  $M = 3$ ,  $N = 9$ ,  $q = 0.07$ ,

$$\vec{v} = \begin{pmatrix} 1 \\ 1.5 \\ 2 \end{pmatrix} \quad (9)$$

are shown on the fifth line of Table 1, while the results for  $q = 0.1$  calculated for two of these cases are shown after the slash.

### 2.2.4 Tailored linear feedback and the generation-specific non-local algorithm

The idea of bi-local control allows excluding undesired changes in the feedback sign determined at an earlier stage of control that may be induced at a later stage. In the feedback matrix Eq.(8), we identify parts that belong to different generations, corresponding to different orders of the parameter  $q$ . The first generation corresponds to  $q^0$ , and the last, the most recent, generation to  $q^{M-1}$ . Evidently, each generation accounts for the feedback at the corresponding time scale. The idea of the control algorithm is that changing the sign of a variable belonging to a generation blocks changes of the signs of the variables belonging to all former generations.

Formally, the bi-local control implies that the set of equations (4,5) is modified by the presence of step factors  $\Theta(Z - z_i)$  at the derivatives for the variables  $z_i$  corresponding to "generations" that happened after

than that of  $i$ , and reads

$$\frac{d}{dt}z_i(t) = \left[ \prod_{r \in \text{inferior}(i)} \Theta(Z - z_r(t)) \right] \left( \frac{dx_i}{dt} \right)^2 \quad (10)$$

$$\frac{d}{dt}x_i = G_{ii} \sum_{j=1}^N \sum_{k=1}^M \beta_{i,k} \alpha_{k,j} x_j$$

$$G_{ii} = \text{sign}(Z - z_i(t)),$$

where  $\Theta(x)$  is the step function. The first equation of this system shows that the functionals  $z_i(t)$  governing the feedback signs are no longer local, since dynamic equations ruling these quantities depend not only on the corresponding local squared velocities but also on the values of the functionals for other variables. This construction further improves the success rate. The results of the numerical work for the success rate  $R_{\text{generations}}$  in this case are shown in the last line of the Table 1 for  $q = 0.07-0.1$ .

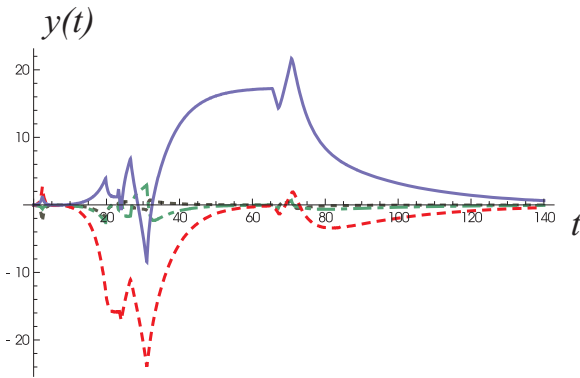


**Fig. 1** An example of stabilizing a four-dimensional subspace in a 40-dimensional space. Time dependencies of the parameters  $y_{1..4}$ , that determine the subspace for  $y_i = 0$  are shown. The first variable  $y_1$  (the blue solid line) corresponds to the first generation of the variables  $x_1 \dots x_{10}$  having the strongest coupling. The second variable,  $y_2$ , (the red dashed line) is coupled to the variables  $x_{11} \dots x_{20}$  with weaker coupling constants, scaled by the factor  $q = 0.4$  with respect to the first variable. The third and the fourth generations (the dash-dot and the dotted lines, green and black, respectively) have couplings scaled by the factors  $q^2$  and  $q^3$ , respectively. In the figure, one can see seven sequential discontinuities of the derivatives of the dependencies related to the changes of signs of the most nimble variables  $x_i$ , that first occurs in the first generation, then in the second, etc. The changes in each of the generations manifest themselves in all dependencies via the matrix  $\hat{\alpha}$

In Fig.1 we show an example of the time dependent deviations  $y_{1..4}(t)$  in the case of a successful control for  $N = 4$ ,  $M = 40$ ,  $q = 0.4$ , where the abrupt changes of the dependencies reflect changes of the feedback signs.

### 2.3 Feedback Strength Exploring Algorithm

The bi-local algorithm can be modified to gain the 100% success rate if instead of the fixed power factors  $q^n$  entering Eq.(8) one allows sequential choosing of these feedback strength parameters for each next generation. In a sense, this algorithm implies learning, that is, given a task  $\hat{\alpha}$ , it modifies the feedback matrix  $\hat{\beta}$  once the sign-changing algorithm does not result in the required subspace stabilization. More specifically, given  $q < 1$ , similar to Eq.(8) where

$$\hat{\beta} = \begin{pmatrix} \vec{v} & 0 & 0 & \dots & 0 \\ 0 & q^{p_1} \vec{v} & 0 & \dots & 0 \\ 0 & 0 & q^{p_2} \vec{v} & \dots & 0 \\ \dots & \dots & \dots & \dots & \dots \\ 0 & 0 & 0 & \dots & q^{p_{M-1}} \vec{v} \end{pmatrix}, \quad (11)$$

the power parameters  $p_1 \leq p_2 \leq \dots p_{M-1}$  that have to be chosen such that the subspace  $\{y_i = 0\}$  is stable.

One begins with all  $p_i = \infty$ , that is, with a one-dimensional subspace, which can always be made stable by proper choice of signs. Next, one sets  $p_1$  to zero, and starts to implement the sign changing algorithm in the subspace of the second diagonal cell of Eq.(13). If this algorithm does not lead to a stable subspace of the dimension 2, one increases  $p_1$  by unity, and implements the sign-changing algorithm for the second cell once again. Repeating this procedure leads to finding  $p_1$  such that the two-dimensional space becomes stable. Next, one turns to the third cell of the matrix Eq.(13), puts  $p_2 = p_1$ , and implements the sign-changing algorithm complemented by augmentation of  $p_2$  by unity, if needed, until the third dimension gets stable. The procedure being sequentially applied to all the cells of Eq.(13), finally yields a feedback matrix  $\hat{\beta}$  stabilizing the required subspace of the dimension  $M$ . for the chosen task matrix  $\hat{\alpha}$ .

For the case of  $N = 100$ ,  $M = 10$ , in Table 2 we present sets  $\{\mathcal{S}_i\}_m$  of the negative real parts  $\mathcal{S}_i$  of the eigenvalues  $c_i$  of the matrix  $\hat{\alpha}\hat{\beta}$  obtained after 10 castings ( $m = 1 \dots 10$ ) for random matrices  $\hat{\alpha}$  and matrices  $\hat{\beta}$  found as a result of implementation of the described algorithm. In Fig.2 we show the average eigenvalues and their mean absolute value deviation from the average calculated with the help of this algorithm. Both these quantities are exponentially decreasing with the eigenvalue number. Note that it does not make sense to put the results of the calculations into Table 1, since the corresponding entries are all unities.

This result means that the local control based on the change of the feedback sign for the most nimble variable (the AMN-rule) combined with a simple non-local

$\{\mathcal{S}_i\}_m \setminus i$	1	2	3	4	5	6	7	8	9	10
$\{\mathcal{S}_i\}_1$	1.59	1.57	1.57	0.00253	0.00253	0.00161	0.00161	0.000144	0.000144	$2.0 \cdot 10^{-5}$
$\{\mathcal{S}_i\}_2$	1.2	0.219	0.219	0.197	0.197	0.187	0.0214	0.0214	$1.69 \cdot 10^{-3}$	$1.69 \cdot 10^{-3}$
$\{\mathcal{S}_i\}_3$	0.849	0.131	0.131	0.0297	0.0297	0.0223	0.0223	$1.51 \cdot 10^{-4}$	$2.3 \cdot 10^{-5}$	$2.3 \cdot 10^{-5}$
$\{\mathcal{S}_i\}_4$	2.86	1.28	1.28	0.317	0.317	0.0807	0.0807	$5.75 \cdot 10^{-3}$	$5.75 \cdot 10^{-3}$	$2.26 \cdot 10^{-3}$
$\{\mathcal{S}_i\}_5$	2.27	0.37	0.37	0.0824	0.0824	$2.46 \cdot 10^{-3}$	$8.38 \cdot 10^{-4}$	$8.38 \cdot 10^{-4}$	$1.24 \cdot 10^{-4}$	$6.33 \cdot 10^{-5}$
$\{\mathcal{S}_i\}_6$	1.48	0.614	0.614	0.411	0.13	0.13	0.109	0.109	0.1	0.1
$\{\mathcal{S}_i\}_7$	3.54	3.54	1.21	1.21	0.208	0.208	0.0317	0.0317	$2.87 \cdot 10^{-3}$	$2.87 \cdot 10^{-3}$
$\{\mathcal{S}_i\}_8$	6.58	0.751	0.27	0.27	0.187	0.187	0.0363	0.0363	0.012	0.012
$\{\mathcal{S}_i\}_9$	1.85	1.85	0.507	0.507	0.0478	0.0478	0.0244	0.0244	$6.83 \cdot 10^{-4}$	$6.83 \cdot 10^{-4}$
$\{\mathcal{S}_i\}_{10}$	0.652	0.652	0.602	0.602	0.138	0.138	0.0734	0.0734	$4.71 \cdot 10^{-3}$	$4.71 \cdot 10^{-3}$

**Table 2** Sets of the negative real parts of the eigenvalues of matrix  $\hat{\alpha}\hat{\beta}$  obtained with the help of the feedback strength exploring algorithm for ten randomly chosen task matrices  $\hat{\alpha}$ .

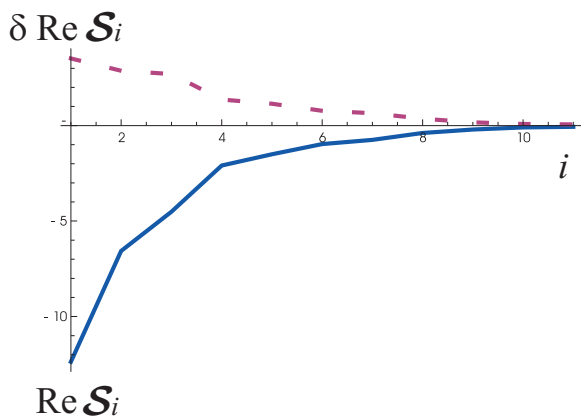


**Fig. 2** The average sorted eigenvalues (solid line) and their average mean absolute value deviation (dotted line) obtained for the case  $N = 143, M = 11$  with the help of the feedback strength-exploring algorithm. The average has been taken over 25 casts of the random matrix  $\hat{\alpha}$ .

control solves the feedback search problem. This nonlocal control requires freezing the feedback parameters for the previous generations once a new generation starts to perform the AMN-rule-based local control. Moreover, it requires a learning procedure with adjusted attenuation of the generation couplings. Though the proposed algorithm solves the problem for any large dimension  $M$ , and thus explicitly demonstrates a possibility to construct a 100% successful algorithm, it may yield the coupling strengths so weak, that the obtained solution has no practical value.

#### 2.4 Susceptibility to Noise Reveals Feedback Structure

We now address the question: What happens with the convergence towards the stabilized subspace ensured by

the feedback matrix

$$\Omega_{i,j} = \text{sign}_i(t \rightarrow \infty) \sum_{k=1}^M \beta_{i,k} \alpha_{k,j} \quad (12)$$

in the presence of noise? Again, as earlier, we emphasize that for physiological systems "noise" implies external task-independent actions that can be of various origin, including both spontaneous changes in intrinsic neural variables and uncontrolled action of an external force field. Here  $\text{sign}_i(t \rightarrow \infty)$  denotes the sign, which results from successful implementation of the control algorithm. We specify this question by asking: How far from the average positions  $x_i(t)$  satisfying the dynamic equations can the actual variables  $X_i(t) = x_i(t) + \delta x_i(t)$  deviate in the presence of a time-dependent noise  $f_i(t)$ ? It can be immediately answered in the basis of the eigenvectors  $\vec{\mathcal{X}}_i$  of  $\Omega_{i,j}$  where  $\vec{x}(t) = \sum_i x_i(t) \vec{\mathcal{X}}_i$ .

One considers the dynamic equations

$$\frac{d}{dt} \delta x_i(t) = \mathcal{S}_i \delta x_i(t) + f_i(t), \quad (13)$$

for the deviations  $\delta x_i(t)$ , where  $\mathcal{S}_i$  denotes eigenvalues of  $\hat{\Omega}$ . The solution

$$\delta x_i(t) = \int_0^t e^{\mathcal{S}_i(t-\tau)} f_i(\tau) d\tau, \quad (14)$$

of this equations in the Fourier representation

$$\delta x_i(\omega) = \frac{1}{\mathcal{S}_i - i\omega} f_i(\omega), \quad (15)$$

suggests that the spectral noise intensity  $|x_i(\omega)|^2$  of the coefficients  $x_i(t)$  is related to the spectral noise intensity  $|f_i(\omega)|^2$  of  $f_i(t)$  via the relation

$$|x_i(\omega)|^2 = \frac{1}{|\mathcal{S}_i - i\omega|^2} |f_i(\omega)|^2, \quad (16)$$

which corresponds to the susceptibility  $|\mathcal{S}_i - i\omega|^{-2}$ .



In order to find the net mean square deviation  $\sqrt{\langle \delta x_i^2 \rangle}$  of the variable  $X_i$ , one has to choose a model for the random perturbing forces or noise. In contrast to the Gaussian noise, typical of physical multi-body systems, due to the central limit theorem of statistics, biological systems may, and usually do manifest other type of noisy behavior, since the underlying processes may emerge from complicated nonlinear and non-random processes developing at the time scales much shorter as compared to the time scale of the process under consideration. The simplest model includes randomly chosen static forces  $f_i$  acting on the relevant variables during a time interval  $T$  and, in each, next time intervals, these forces show random values. This yields

$$|f_i(\omega)|^2 = \left( \frac{\sin \frac{\omega T}{2}}{\omega T} \right)^2 |f_i|^2, \quad (17)$$

and hence

$$\begin{aligned} \langle \delta x_i^2 \rangle &= |f_i|^2 \int \frac{d\omega}{2\pi} \frac{1}{|\mathcal{S}_i - i\omega|^2} \left( \frac{\sin \frac{\omega T}{2}}{T\omega} \right)^2 \\ &= |f_i|^2 \frac{\text{Re} [(e^{\mathcal{S}_i T} - 1) \mathcal{S}_i^{-2}]}{T \text{Re} \mathcal{S}_i}. \end{aligned} \quad (18)$$

Average square variances  $\langle \delta x_i^2 \rangle$  of the independent modes correspond to eigenvalues  $\mathcal{C}_i$  of the covariance matrix, when one considers the problem in a basis, different from  $\{\vec{\mathcal{X}}_i\}$ .

For the case  $\mathcal{S}_i = 0$  one should take into account a finiteness of the evolution time interval  $\mathcal{T}$  and replace  $\mathcal{S}_i$  by  $i/\mathcal{T}$ , thus obtaining the net mean squared deviation diffusively rising with time

$$\langle \delta x_i^2 \rangle \sim \mathcal{T}/T. \quad (19)$$

Noise analysis may serve as a powerful tool of revealing the eigenvectors of the matrix  $\Omega_{i,j}$  of Eq.(12), which via the Eqs.(16,17), also gives some ideas about magnitudes of the corresponding eigenvalues for a reasonably chosen model of the noise. One needs to calculate the noise covariance matrix  $C_{ij} = \langle \delta x_i \delta x_j \rangle$  from the experimentally observed deviations of the running measured values from their average values in the stationary regime. Eigenvectors  $\vec{\mathcal{X}}_i$  of this matrix should coincide with those of  $\hat{\Omega} = \hat{G}(t \rightarrow \infty) \hat{\beta} \hat{\alpha}$ . Moreover, this method can also be employed for determining the eigenvalues of the time-dependent values of the feedback matrix  $\hat{\Omega}(t) = \hat{G}(t) \hat{\beta} \hat{\alpha}$ , provided the time intervals where this object changes significantly are long enough and exceed a typical correlation time of the noise.

Note that for the case  $N > M$ , the non-zero eigenvalues of the  $N \times N$  matrix  $\hat{\Omega} = \hat{G} \hat{\beta} \hat{\alpha}$  coincide with  $M$

eigenvalues of the  $M \times M$  matrix  $\hat{\omega} = \hat{\alpha} \hat{G} \hat{\beta}$ . The remaining  $N - M$  eigenvalues are zeros, unless an additional requirement is imposed on the matrix  $\hat{\Omega}$ . Spread of the variations  $\delta x_i^2$  in the directions of the corresponding eigenvectors are expected to be large and be governed by the spectral properties of the noise. In other words, given a task matrix and a feedback matrix, which has been found with the help of the stabilization search algorithm, there exist two subspaces in the space of the variables  $x_i$ , the so-called uncontrolled manifold (UCM)[27] and its orthogonal complement (ORT) also sometimes addressed as the null-space and the range-space, respectively. ORT is the task-specific subspace expected to show high stability, which implies that variance in ORT is expected to be small. In the UCM, variance is generally expected to be large and increasing with time, unless there are other factors, outside the explicit task formulation, that keep it within a certain range. In fact, after a person becomes an expert in a motor task, repetitive attempts at the task lead to variable combinations of elemental variables that all lead to successful task performance within a permissible error margin ([4]; reviewed in [15]). However, not all possible combinations of the involved elemental variables are used across repetitive attempts. Such self-imposed additional constraints may be addressed as 'perfectionism'; they may reflect optimization with respect to a cost function (e.g., [36]). Figure 3 illustrates the task  $x_1 + x_2 = C$  for different values of  $C$ . While all points on the slanted dashed lines correspond to perfect task performance, actual behavior shows much more constrained clouds of solutions that show larger deviations along the solution space (the UCM) compared to deviations orthogonal to that space (that lead to errors in performance). Note that if the task is learned for a particular value of  $C$ , the solutions show robustness: Similar relative locations and shapes of the solution clouds for other values of  $C$ .

More formally, assuming a feedback matrix  $\hat{\beta}$  stabilizing a  $M$ -dimensional subspace is found, one may think of imposing complementary constraint, that can either be in the form of explicit equations or follow from a requirement of minimization of a cost function. In such a setting, one speaks about stabilization of a subspace of a dimension  $M_+$  exceeding the dimensionality  $M$  of the initial task subspace. Such perfectionism may be viewed as a secondary tasks decreasing variance in some directions of the UCM.

We would like to emphasize once again that there exists three types of specific bases that can be employed for the dynamics description: (1) A laboratory basis of measured variables, (2) A basis of modes resulting from both body- and task-imposed constraints, while each

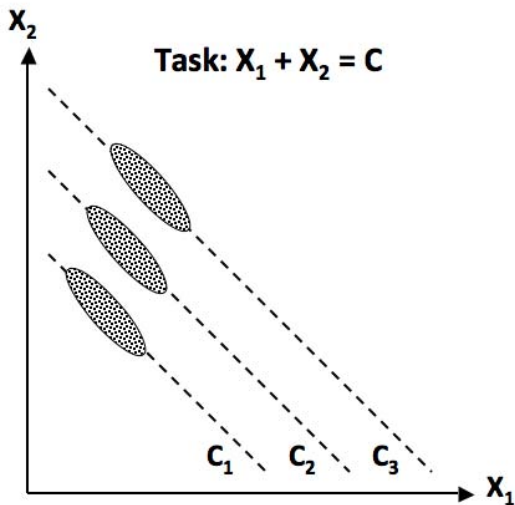


**Fig. 3** Consider a task of producing a constant sum of two variables, e.g., pressing with two fingers and producing a constant total force level. The dashed lines show solution spaces (uncontrolled manifolds, UCMs) for three different force levels,  $C_1$ ,  $C_2$ , and  $C_3$ . Across repetitive trials, clouds of data points form ellipses elongated along the corresponding UCM. This shape reflect lower stability along the UCM as compared to the orthogonal direction relevant to the task-imposed constraint. Note that the three data clouds are centered not randomly along the UCMs but reflect a certain preferred sharing of the task between the two effectors. This preference may reflect an optimization principle.

mode has independent noise statistics, and (3) A task-specific basis of variables along which the control is local. The last basis is a conceptually new feature affording a simple structure of the control algorithm.

The relation between the second and the third bases may change during the process of stability search: Application of the local control  $\hat{G}$  leads to a change of  $\hat{\omega} = \hat{\alpha}\hat{G}\hat{\beta}$ , that is, the way the task requirement  $\hat{\alpha}$  is mapped onto the feedback action. Thereby it may affect both the basis of the noise-decorrelated modes and the magnitude of the corresponding modes susceptibilities. There exists such an extreme, where the mode susceptibilities  $|\mathcal{S}_i - i\omega|^{-2}$  vary without changing the corresponding eigenvectors  $\vec{\mathcal{X}}_i$  of  $\hat{\Omega}$  – the linear combinations  $\vec{\mathcal{X}}_i$  and  $\vec{\mathcal{X}}_j$  of the laboratory basis variables remain statistically independent, and only the variance  $\langle \delta x_i^2 \rangle$  of one combination starts to exceed that of the other  $\langle \delta x_j^2 \rangle$ . One can call this regime "mode crossing", by the analogy to the phenomenon of "term crossing" in Quantum Mechanics [1]. In the general case where, along with a change of the susceptibilities, the local changes equally result in the emergence of an appreciable covariance between the modes  $\langle \delta x_i \delta x_j \rangle \neq 0$ , one encounters the phenomenon of so-called "avoid crossing",

where formerly the larger mode susceptibility, though approaching in magnitude the other one, remains always larger, while both eigenvectors  $\vec{\mathcal{X}}_i$  and  $\vec{\mathcal{X}}_j$  corresponding to these modes rotate.

## 2.5 Algorithm for Hierarchical Feedback

Hierarchical control considered in this section gives an example of stabilization search algorithm different from that considered earlier. We demonstrate that such an algorithm requires only local control, whereas the role of nonlocal control can be played by another randomly chosen linear feedback matrix once the current one does not yield stabilization. The idea of hierarchical control of the human body is very old. Arguably, the first hierarchical system considered the brain and the spinal cord. A comprehensive scheme of control with referent configurations has been suggested recently built on a hierarchical principle, starting with referent values for a few task-specific, salient variables, and resulting in referent length values for numerous involved muscles [16]. An example of hierarchical control is the command structure of an army, where a general gives orders to privates through the commanders of regiments, battalions, and platoons. We explore efficiency of hierarchical control in this section, along with another modification – the most nimble  $x_i$  is no longer punished by a step change of the sign of its contribution but experiences a smooth change of the participation in the feedback as the cosine of the corresponding functional  $z_i$ .

### 2.5.1 Intrinsic instability of the hierarchical control

In mathematical terms, the time derivative of a vector  $\vec{x}_n$  of variables at  $n$ -th step depends on the variables  $\vec{x}_{n-1}$  at the previous step, while the spatial dimension  $N_n$  of each next step varies from step to step. At each step local control may be implemented. For example, the corresponding set of the local control equations for a three-level hierarchy has the form

$$\vec{y} = \hat{\alpha} \vec{x}_3 \quad (20)$$

$$\begin{aligned} \frac{d}{dt} x_{1i} &= (\hat{G}_1)_{ii} (\hat{A} \vec{y})_i \\ \frac{d}{dt} x_{2i} &= (\hat{G}_2)_{ii} (\hat{B} \vec{x}_1)_i \\ \frac{d}{dt} x_{3i} &= (\hat{G}_3)_{ii} (\hat{C} \vec{x}_2)_i, \end{aligned}$$

based on the diagonal matrix elements

$(\hat{G}_n)_{ii} = \cos [z_{ni}(t)]$  of the local control operators  $\hat{G}_n$ . If at each level  $n$  of the hierarchy, we also include diagonal damping matrices  $\hat{\gamma}_n$  of the dimension given by

the number  $N_n$  of the variables at this level, the set of equations (20) can be seen as a single matrix equation

$$\begin{pmatrix} \left(\frac{d}{dt} - \hat{\gamma}_1\right) \vec{x}_1 \\ \left(\frac{d}{dt} - \hat{\gamma}_2\right) \vec{x}_2 \\ \left(\frac{d}{dt} - \hat{\gamma}_3\right) \vec{x}_3 \end{pmatrix} = \begin{pmatrix} \hat{G}_1 & 0 & 0 \\ 0 & \hat{G}_2 & 0 \\ 0 & 0 & \hat{G}_3 \end{pmatrix} \begin{pmatrix} 0 & 0 & \hat{A}\hat{\alpha} \\ \hat{B} & 0 & 0 \\ 0 & \hat{C} & 0 \end{pmatrix} \begin{pmatrix} \vec{x}_1 \\ \vec{x}_2 \\ \vec{x}_3 \end{pmatrix}. \quad (21)$$

Alternatively, the local control operation may be applied not to susceptibility of a given variable to external factors, but to efficiency with which this variable acts on the variables of the next generation. In such a case, two operators on the left hand side of Eq.(21) have to be interchanged

$$\begin{pmatrix} \left(\frac{d}{dt} - \hat{\gamma}_1\right) \vec{x}_1 \\ \left(\frac{d}{dt} - \hat{\gamma}_2\right) \vec{x}_2 \\ \left(\frac{d}{dt} - \hat{\gamma}_3\right) \vec{x}_3 \end{pmatrix} = \begin{pmatrix} 0 & 0 & \hat{A}\hat{\alpha} \\ \hat{B} & 0 & 0 \\ 0 & \hat{C} & 0 \end{pmatrix} \begin{pmatrix} \hat{G}_1 & 0 & 0 \\ 0 & \hat{G}_2 & 0 \\ 0 & 0 & \hat{G}_3 \end{pmatrix} \begin{pmatrix} \vec{x}_1 \\ \vec{x}_2 \\ \vec{x}_3 \end{pmatrix}. \quad (22)$$

Though offering a simple way to address many variables at once, hierarchical control may add instability. Therefore, the intermediate steps have to be damped in order to avoid such an instability in contrast to one-step control of Eq.(10). In particular, note that for zero damping  $\hat{\gamma}_i = 0$ , even the simplest two-level control becomes unstable, and this is always the case for a higher number  $l$  of the control levels. The root of this instability is rather simple, and can be illustrated with an example of a three-level control scheme, with just one variable at each level, when Eq.(21) takes the form

$$\begin{aligned} \frac{d}{dt}x_1 &= G_1 A \alpha x_3 \\ \frac{d}{dt}x_2 &= G_2 B x_1 \\ \frac{d}{dt}x_3 &= G_3 C x_2 \end{aligned} \quad (23)$$

corresponding to the characteristic equation

$$\lambda^3 = G_3 C G_2 B G_1 A \alpha. \quad (24)$$

It is evident that, whatever a non-zero complex number standing on the right hand side of this equation is, the phase factors of the three roots of the cubic equation are equally distributed on the unit circle in the complex plane such that at least one of them has a positive real part. The same structure of the root distribution persists in a higher-dimensional case with  $l$ -level control, since the characteristic equation in this case has the form

$$\text{Det} \left| \lambda^l - \hat{G}_l \dots \hat{G}_3 \hat{C} \hat{G}_2 \hat{B} \hat{G}_1 \hat{A} \hat{\alpha} \right| = 0, \quad (25)$$

and hence the roots of the characteristic polynomial given by  $l$ -th roots of the eigenvalues of the matrix  $\hat{G}_l \dots \hat{G}_3 \hat{C} \hat{G}_2 \hat{B} \hat{G}_1 \hat{A} \hat{\alpha}$  are also uniformly distributed on the corresponding circles in the complex plane, with radii given by the eigenvalues moduli.

We thus come to the conclusion that damping is indispensable for stable hierarchical control. At the same time, all  $\hat{\gamma}_i > 0$  imply a trivial asymptotic situation of completely damped motion at all levels for all tasks. Therefore, in order to have a reasonable model, we have to assume vanishing of the damping rates at only one hierarchical level of control. Presumably, this level should have the maximum dimensionality  $N_n$ .

### 2.5.2 Action of the feedback loops

We note that stability can be to a certain extent improved by introducing intermediate feedback loops to the net feedback loop as shown in Fig.4.

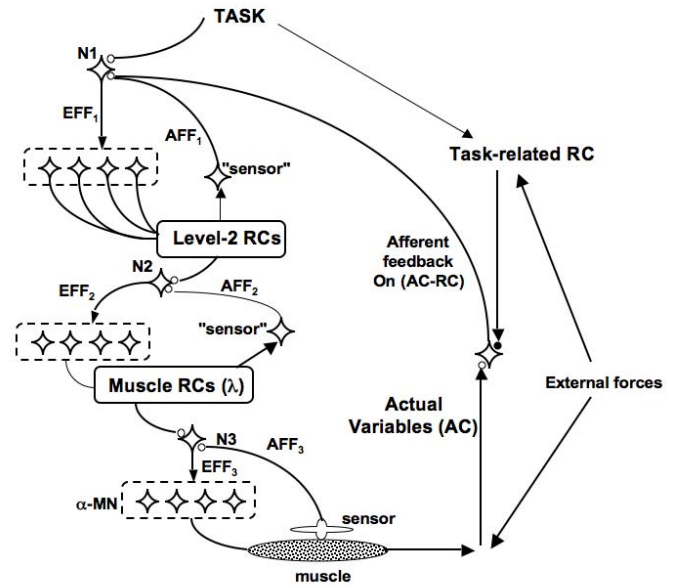


**Fig. 4** A scheme of hierarchical control of the hand within the idea of control with referent configurations (RCs) of the body[10]. At the top level, a low-dimensional set of referent values for salient, task-specific variables is reflected in the RC. A sequence of few-to-many transformations results in higher-dimensional RCs at the digit level and muscle level. Local feedback loops ensure stability with respect to the variables specified by the input. The global feedback loop ensures that the actual body configuration moves towards one of the solutions compatible with the task RC. At each level, inputs to a neuronal pool ( $N1, N2$ , and  $N3$ ) are combined with afferent feedback (AFF) to produce the output (efferent signals, EFF). At the lowest level, elements are alpha-motoneurons and their referent coordinates correspond to the thresholds of the tonic stretch reflex (lambda). Modified by permission from [16].

For the example of aforementioned three-level hierarchical control, the Laplace-transformed equations of motion for the case of feedback loop equipped with secondary feedback loops read

$$\begin{aligned}\lambda \vec{x}_1 &= \widehat{G}_1 \widehat{A} \widehat{\alpha} \vec{x}_3 + \widehat{A}_2 \vec{x}_2 \\ \lambda \vec{x}_2 &= \widehat{G}_2 \widehat{B} \vec{x}_1 + \widehat{A}_3 \vec{x}_3 \\ \lambda \vec{x}_3 &= \widehat{G}_3 \widehat{C} \vec{x}_2\end{aligned}\quad (26)$$

where the secondary feedback loops of the second and the third hierarchical levels are given by the matrices  $\widehat{A}_2$  and  $\widehat{A}_3$ , respectively. The latter can be also considered as dependent on local variables  $z$ . For a given set of variables  $z$ , the instantaneous eigenvalues  $\lambda$  can be calculated as the roots of an analog of Eq.(25), which reads

$$\text{Det} \left| \lambda - \widehat{G}_3 \widehat{C} \frac{1}{\lambda - \widehat{G}_2 \widehat{B} \widehat{A}_3} \widehat{G}_2 \widehat{B} \frac{1}{\lambda - \widehat{G}_1 \widehat{A} \widehat{A}_2} \widehat{G}_1 \widehat{A} \widehat{\alpha} \right| = 0.$$

Note that in the basis where the matrices  $\widehat{G}_2 \widehat{B} \widehat{A}_3$  and  $\widehat{G}_1 \widehat{A} \widehat{A}_2$  are diagonal, they can be interpreted as damping matrices  $\widehat{\gamma}_1$  and  $\widehat{\gamma}_2$ , respectively, although in this case these matrices are dependent on parameters  $z$ , which, generally speaking, in this representation cannot be considered as local control. Still, this brings about an idea of the self-adjusting damping dependent on time via the parameters  $z_i(t)$ .

### 2.5.3 Stabilization by self-adjusting damping

Adjusting gain in the feedback loops controls stability at each hierarchical level. This effect can be modeled when the damping parameters  $\gamma_i$  are taken depending on the local parameters  $z_i$ , increasing, for instance, as

$$\gamma_i = \Gamma_i + \mu_i z_i \quad (27)$$

, for the variables at each damped level. The parameters  $\gamma_i$  are positive for all but one hierarchical levels, where they may remain zero, in order to avoid the trivial case of complete damping of all variables. An analog of the characteristic equation (25) for this case gets simplified and reads

$$\text{Det} \left| \lambda - \widehat{\gamma}_3 - \widehat{G}_3 \widehat{C} \frac{1}{\lambda - \widehat{\gamma}_2} \widehat{G}_2 \widehat{B} \frac{1}{\lambda - \widehat{\gamma}_1} \widehat{G}_1 \widehat{A} \widehat{\alpha} \right| = 0,$$

where one of the three diagonal matrices  $\widehat{\gamma}_1$ ,  $\widehat{\gamma}_2$  or  $\widehat{\gamma}_3$  is assumed to be zero.

In turn, for the local control over the damping rate, the dependence  $z_i(t)$  can be given by a differential equation relating the positive rate of increase  $\frac{d}{dt} z_i$  with an even power  $f$  of either the corresponding variable,

$$\frac{d}{dt} z_i = \epsilon (x_i)^f, \quad (28)$$

or the corresponding variable velocity,

$$\frac{d}{dt} z_i = \epsilon \left( \frac{dx_i}{dt} \right)^f, \quad (29)$$

where  $\epsilon < 1$  is a numerical parameter, which may depend on the hierarchy level number and the variable number.

In the following Table 3 we present the success rates calculated for series of 100 random casts of the rectangular feedback matrices  $\widehat{A}$ ,  $\widehat{B}$ , and  $\widehat{C}$  corresponding to the dimensions  $N_1$ ,  $N_2$ , and  $N_3$  of the spaces of  $x_1$ ,  $x_2$ , and  $x_3$ , respectively, and generated independently each time for a random cast of the  $N_3 \times M$  task matrix  $\widehat{\alpha}$ . The identical damping parameters  $\Gamma_i = 0.1$  and  $\mu_i = 1$  have been chosen. Moreover, in order to avoid the trivial situation yielding 100% success rate, where all variables get strongly damped and hence become vanishing in the course of time, a fourth hierarchical level corresponding to the vector variables  $\vec{x}_0$  defined by the differential equation without damping,  $\frac{d}{dt} \vec{x}_0 = \vec{y}$ , has been included into Eq.(23). The non-zero diagonal matrix elements of the local feedback control matrices  $\widehat{G}_{1,2,3}$  have been chosen here as  $G_{ii} = \cos(0.1z_i)$ , and the power index  $f$  and the numerical parameter  $\epsilon$  in Eq.(29) have been chosen equal to 4, and 0.1, respectively for all variables.

A typical time dependence  $\vec{y}(t)$  for the successfully stabilized subspace is shown in Fig.5 (the top plot). In accordance with the smoothness of the local feedback control dependence ( $\cos(0.1z_i)$  instead of  $\text{sign}(10\pi - z_i)$ ), the time dependence does not manifest a cusp-like changes of the derivatives, typical of those seen in Fig.1. For unsuccessful control, the dependence looks like the one depicted in Fig.5 (the bottom plot).

A rather high success rate of the hierarchical local control over the dynamics for random choice of the feedback matrices and self-adjusting damping suggests a strategy, which can replace the non-local control. Once the current random cast of the feedback matrices does not yield stabilization during a run, one may achieve it by taking another random cast in the course of the same run, and in case of failure, repeat the attempt again and again. In particular, the probability 0.3 implies that just a few (4–5) such casts during a run are required in order to stabilize a 5-dimensional subspace. Changing the entire linear feedback matrices when the local control turns out to be inefficient may be considered as an action replacing nonlocal control discussed in the previous section.

Note, that the dimensionality at each step of the hierarchy does not need to be larger than the dimensionality of the previous step. We illustrate this by an example of control over a two-dimensional space  $y$  exerted

$M$	1	2	3	4	5	6
$N_1/N_2/N_3$	5/50/200	5/50/200	5/50/200	5/50/200	5/50/200	6/50/200
$R$	1	1	0.69	0.43	0.3	0.15

**Table 3** The stabilization success rate of a  $M$ -dimensional subspace for hierarchical control with  $N_1/N_2/N_3$ -dimensional levels.

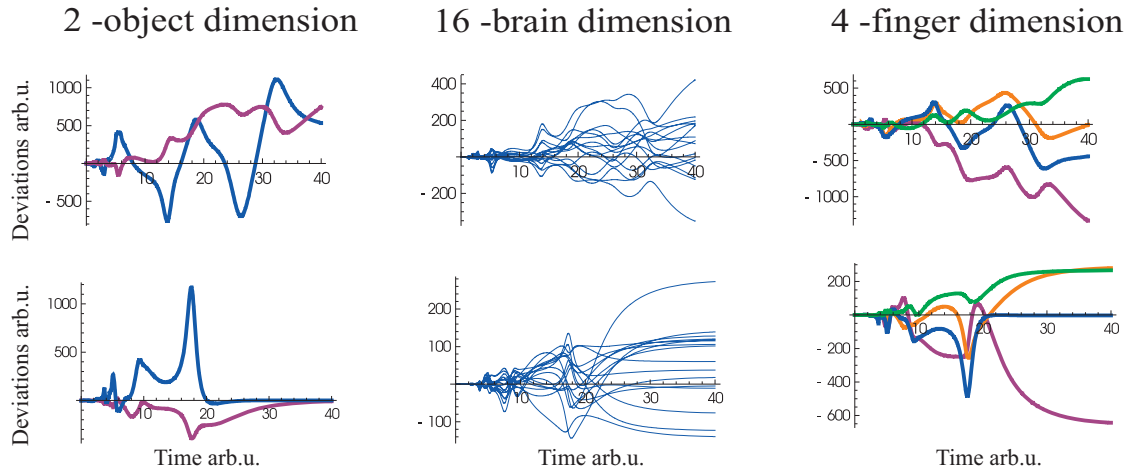


**Fig. 6** Examples of successful (lower panels) and unsuccessful (upper panels) search for the new equilibrium control. We show coordinate variables as functions of time in arbitrary units. First column: deviations of two controlled coordinates from their prescribed value – zero. The second column: dynamics of the hypothetical elemental variables tend to some asymptotic values for the successful control. Third column: dynamics of motor variables. One sees the dynamics of transition from the old equilibrium position to the new one.

by a three-step hierarchical feedback with locally changing parameters. The first-step variables  $\vec{x}_1$  belong to a space of the dimension  $N_1 = 4$ ; here the damping increases according to Eqs.(27,29) with  $\epsilon = 0.2$ ,  $f = 2$ , and  $\mu_i = 0.1$ . Next step of the hierarchy comprises the variables  $\vec{x}_2$  that belong to a space of the dimension  $N_2 = 16$  where they experience no damping. The last step of the hierarchic feedback comprises variables  $\vec{x}_3$  in a four-dimensional space,  $N_3 = 4$ , with strong constant damping  $\Gamma_i = 5$  at the third level. The success rate for these parameters was  $R \simeq 0.8$ . Examples of unsuccessful and successful search of stability are shown in Fig.6 for the components of the vectors  $y$ ,  $\vec{x}_2$ , and  $\vec{x}_3$ . One sees that for successful control the components of the high-dimensional vectors tend to asymptote with time, while for unsuccessful control, they keep changing.

### 3 Experiments with Human Hand

An experiment was performed to illustrate one of the central ideas of the suggested scheme and check some of its predictions. We used the task of accurate force and moment-of-force production by the four fingers of the dominant hand. The forces produced by four fingers, the index, the middle, the ring, and the little,

were controlling the position of a point on the computer screen. Two types of perturbations were used. First, we modified the visual feedback leading to changes in the mapping between the finger forces and the two task variables. Second, we used mechanical perturbations applied to a finger that led to actual changes in the two task variables. The experiments were approved by the Office for Research Protections at the Pennsylvania State University.

#### 3.1 Visual Feedback Perturbation

The first experiment was as follows. Four 6-axis force/moment sensors (Nano-17, ATI Industrial Automation, USA) mounted on the table were used to measure normal forces produced by the tips of the index ( $I$ ), middle ( $M$ ), ring ( $R$ ), and little ( $L$ ) fingers. To increase friction between the digits and the sensors, 320-grit sandpaper (SandBlaster, 3M, USA) was placed on the contact surfaces of the sensors. The centers of the sensors were evenly spaced at 30 mm. The output analog signals from the sensors were digitized with the 16-bit data acquisition card (PCI-6225, National Instrument, Austin, TX, USA) at 100 Hz. A LabVIEW program (LabVIEW 2011, National Instrument, USA) was used to provide visual feedback and store the data on the

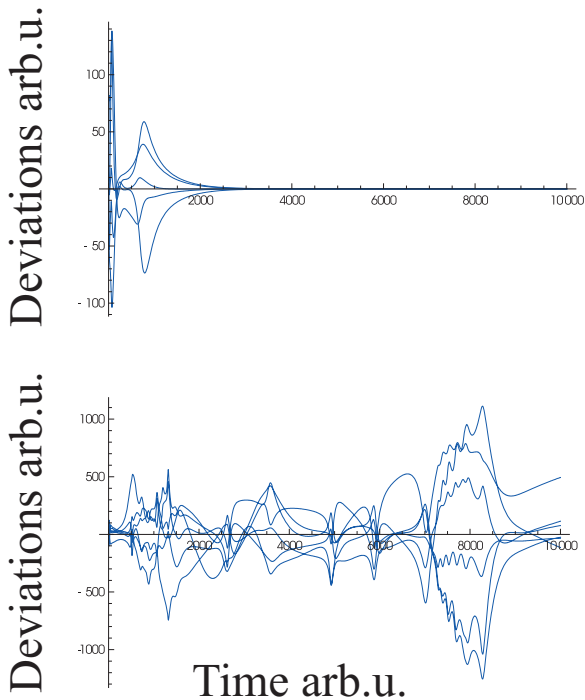


**Fig. 5** Time dependencies for the successfully controlled five-dimensional subspace in the hierarchical cascade setting with  $N_1/N_2/N_3 = 5/50/200$  (upper). Unsuccessful control (lower).

computer (Dell Inc., USA). Offline processing and analysis was done in Matlab (MathWorks, USA).

At the beginning, the four-dimensional space of the finger forces was mapped onto the two-dimensional space of the screen according to a very natural rule - the vertical coordinate was proportional to the net resultant finger force, while the horizontal displacement was given by the net moment of the finger forces computed with respect to a horizontal axis passing in the anterior-posterior direction in-between the R and M finger sensors. The subject was first requested to place the cursor into a position in the middle of the screen and, second, to keep it in this position at all times. Once this task was accomplished, the law according to which the deviation of the finger forces from the steady-state finger force values are mapped to the deviation of the point from the center of the screen was changed without the subject's knowledge. The new law relating the four-dimensional space of the force deviations with the two-dimensional space of the cursor deviations from the center point was given by a new, randomly chosen,  $2 \times 4$  Jacobian matrix. This law drew the system to an unstable regime. In order to keep the point at the center of the screen, the subject had to find a new feedback rule stabilizing this position. Trajectory of the forces exerted by the fingers in the course of this search for new stability were recorded.

### 3.1.1 Results - manifestations of the feedback changes

In Fig.7 we present an example of the time profiles of the finger forces (upper panel), along with the coordinates of the point on the screen (lower panel), which were recorded during a successful trial. Overall stabilization success rate was  $R \simeq 0.55$ .

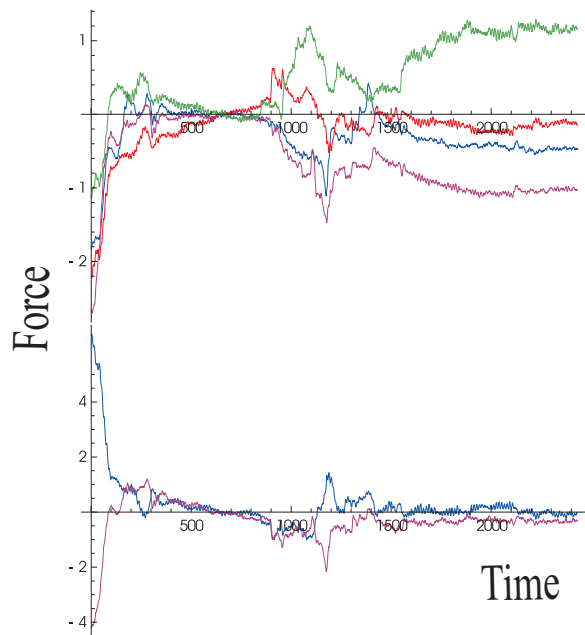


**Fig. 7** Finger forces in  $N$  as functions of time in  $10^{-2}s$  (upper panel) and the coordinates of the point position on the screen (lower panel). The law relating the forces to the position of the point was changed at  $t = 7s$ , and the values of the finger forces at that time were chosen as zero  $N$ .

There is a qualitative similarity between the dependencies depicted in Fig.7 and the corresponding calculated dependencies illustrated in Fig.6.

The sharp spikes and jumps on the experimental curves correspond to changes of the trends; these events show approximately the moments of time when a correcting action was taken similarly to the simulated curve in Fig.1. Though spikes in the simulated curves may be unambiguously associated with the correcting actions of the feedback sign change, within the experimental finger force curves analysis there is no formal rules allowing to identify such moments, and one can speak only about an intuitive similarity between the dependencies. Moreover, since we are exploring the regime of searching for an equilibrium in new, formerly unknown, conditions, we cannot invoke the powerful tool of statistical analysis comparing different trials, since each new trial corresponds to new initial and task conditions, whereas multiple sequential repetitions of the



same experimental setting for the same subject would likely involve processes of learning and adaptation that are beyond the scope of questions addressed here. Still certain information about the moments of changes of the feedback matrix can be extracted from the analysis of noises, since, as discussed in Sect.2.4, the principle axes of the tensor susceptibility to noise (so-called principle components) coincide with eigenvectors of the dynamic matrix  $\widehat{\Omega}$ , and when directions of these axes change, the matrix  $\widehat{\Omega}$  changes as well, thus implying a change of the feedback matrix. Moreover, the larger the eigenvalue  $\mathcal{C}_i$  of  $\widehat{\Omega}$  is, the smaller is the susceptibility of the corresponding direction to noise, in accordance with Eq.(16). The noise analysis is discussed in the next section.

### 3.1.2 Analysis of the principal components of noise covariance reveals feedback changes

Human fingers are not independent force generators: When a person tries to press with one finger, other fingers of the hand show unintentional force increase [13,19]. This phenomenon has been addressed as enslaving or lack of finger individuation [44,26]. Patterns of enslaving are person-specific and relatively robust; changes in these patterns have been reported with specialized practice [34,?]. These patterns may be described as eigenvectors of enslaving  $\vec{f}_{E,i} = \{f_j\}_{E,i}$ , where  $i = \{I - \text{index}; M - \text{middle}, R - \text{ring}, \text{ and } L - \text{little}\}$  stands for an instructed finger. Directions of  $\vec{f}_{E,i}$  may be viewed as preferred directions in the space of finger forces when the person is trying to press with individual fingers They are related as

$$\vec{f}_{E,i} = \widehat{U} \vec{X}_i \quad (30)$$

to the forces  $X_i$  of the individual fingers  $i$  by an orthogonal matrix  $\widehat{U}$  representing rotation in the four-dimensional space. We assume, that these very directions may change during the search of stability and they manifest statistically independent fluctuations thus being the eigenvectors  $\vec{X}_i$  of the deviation covariance matrix.

Since in our experiment the task was formulated in a two-dimensional space, and hence the rank of the dynamic problem presumably equals two, there should be only a two-dimensional sub-space in the space of the finger forces that governs the dynamics of the point on the screen. This implies that only two out of four eigenvalues of the matrix  $\widehat{\Omega}$  differ from zero, and the other two vanish, unless an external to the task requirement associated with additional constraints is imposed upon the system, as mentioned at the end of Sect.2.4. In the latter case, all the eigenvalues do differ from zero, but

they are decreasing exponentially with each next eigenvalue being scaled, on average, by a factor, as it was the case for the hierarchy of nimbleness shown in Fig.2. This has a consequence important for the noise analysis: The directions that belong to the two-dimensional subspace relevant to feedback are less susceptible to noise, while the noisy directions correspond to the null-space and do not contribute significantly to the feedback.

The dependence  $X_i(n)$  of the forces produced by the I, M, R, and L fingers was captured at the sequential time points  $t = n\tau$  separated by time intervals of  $\tau = 10^{-2}$  sec. The covariance matrix was extracted from these experimental data in several steps. First, for each  $X_i(n)$  an average time dependence  $x_i(n) = x_i(t)$  has been calculated numerically as

$$x_i(t) = \sum_n \frac{X_i(n)}{Y\sqrt{\pi}} \exp\left[-\frac{(t-n)^2}{Y^2}\right], \quad (31)$$

where  $\tau$  is chosen as a time unit, while the averaging is performed over a time window  $\sim Y\tau$  with a width  $Y$ . Next, the covariance of the finger forces

$$C_{i,j}(t) = \sum_n \frac{\delta x_i(n)\delta x_j(n)}{Y\sqrt{\pi}} \exp\left[-\frac{(t-n)^2}{Y^2}\right], \quad (32)$$

where

$$\delta x_i(n) = X_i(n) - x_i(n),$$

was found numerically with the same Gaussian width  $Y$ .

Being a real and symmetric matrix,  $C_{i,j}$  can be set in a diagonal form by an orthogonal transformation given by a rotation matrix  $U_{i,j}(t)$  and its inverse matrix  $U_{i,j}^{-1}(t)$ , such that

$$C_{i,j}(t) = \sum_k U_{i,k}(t) \mathcal{C}_k(t) U_{k,j}^{-1}(t). \quad (33)$$

The eigenvalues  $\mathcal{C}_k(t)$  provide us with the principle components of the noise in the orthogonal directions of statistically-independent modes, while the matrix  $U_{i,k}(t)$ , which in the laboratory basis can be viewed as a row of the column eigenvectors  $\vec{X}_i(t)$ , relates these modes to the individual finger variables. All these quantities were found numerically from the data obtained for  $C_{i,j}(t)$ . Note that thus obtained orthogonal matrix  $U_{i,k}(t)$  experiences a time evolution corresponding to rotation in the 4-dimensional space of the finger forces, while the angular velocity of this rotation can be found as the eigenvalues of the left logarithmic derivative of  $U_{i,k}(t)$  defined as

$$\widehat{R}(t) = \frac{1}{i} \frac{\partial \widehat{U}}{\partial t} \widehat{U}^{-1}. \quad (34)$$

The eigenvalues  $R_i$  of  $\hat{R}(t)$  are real and have pairwise opposite signs, such that only two real numbers characterize rotation in the four-dimensional space. We calculate these quantities replacing the derivative in Eq.(34) with the finite difference between two neighboring integer time points. In order to get rid of the so-called shot noise, which is an error-inducing influence of such a replacement, the calculation must be followed by averaging over a time interval shorter than  $Y$ .

Results of such processing of the experimental data presented in Fig.7 are shown in Fig.8.

One can identify eleven rotations of the covariance matrix basis  $\vec{\chi}_i(t)$  presumably associated with changes of the feedback matrix. Note that the highest rotation velocity does not necessarily produce a strong effect on the finger forces, since the relevant quantity rather corresponds to the spike area, representing the rotation angle. The situation has much in common with dynamics of so-called adiabatic and diabatic molecular term crossings, well-known in Quantum Mechanics[1]. The maximum rotation velocity corresponds to the time moments when two or several eigenvalues of the matrix have a tendency to coincide, thus getting rid of the difference between the large noise typical of the null-space and small noise typical of the orthogonal subspace in a stationary regime.

### 3.2 Experiments with Mechanical Perturbations

The results of the first experiment have demonstrated qualitative consistency of the model and the experiment. Still the main assumption of the suggested stable control search algorithm, the principle “act on the most nimble one” (AMN) requires additional arguments. The second experiment was designed to test this very principle. Mechanical perturbations (lifting and lowering a finger) were applied during the performance of an accurate multi-finger steady-state task. According to our scheme, quick reactions to these perturbations are based on the AMN rule. We checked this prediction by comparing the directions of changes in the finger force space produced by unexpected perturbations of the steady-state force patterns (described as a vector  $\vec{f}_{P,i}$ ) with the first identifiable correction produced by the subjects (a correction vector,  $\vec{f}_{C,i}$ ). We expected the angle between  $\vec{f}_{C,i}$  and  $\vec{f}_{P,i}$  to be small, smaller than the angle between  $\vec{f}_{C,i}$  and  $\vec{f}_{E,i}$ , defined by Eq.(30).

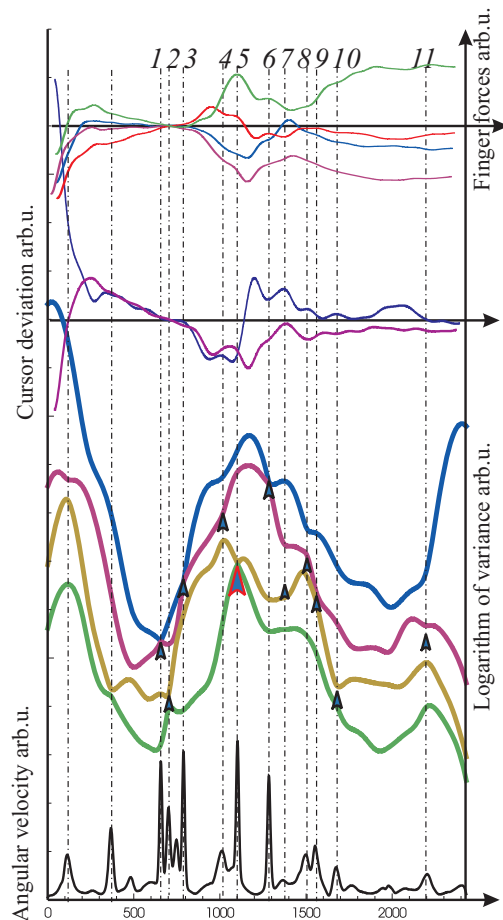


**Fig. 8** The angular velocity  $R_1(t)$  of rotation of the basis of the covariance matrix eigenvectors as function of time (bottom, solid line, arbitrary units). Logarithms of the eigenvalues  $C_k(t)$  of the covariance matrix (four bold curves above the velocity). The average of the covariance matrix was computed over  $Y = 100$  sequential time points with the interval of  $10^{-2}$  sec between the points. The switching of the feedback eventually took place at the domains of “avoid crossings” discussed at the end of Sect.2.4, marked here by arrows, and corresponding to the maxima of the angular velocity. On the top of the plots, the finger forces and the cursor coordinates, corresponding to the dependencies in Fig.7 averaged over the same time intervals  $Y = 100$ , are shown for comparison. The “avoid crossing” of the three eigenvalues occur for the 4-th, 7-th, and 8-th intersections. The strongest contribution comes from the 5-th crossing, which presumably is relevant to changing of the direction in the two-dimensional orthogonal subspace.

#### 3.2.1 Methods - the “inverse piano” setup

Eight young, healthy subjects took part in the experiment (four males). They were right-handed, had no specialized hand training (such as playing musical instruments) and no injury to the hand.

An “inverse piano” apparatus was used to record finger forces and produce perturbations. The apparatus has four force sensors placed on posts powered by



linear motors, which could induce motion of the sensors along their vertical axes (for details see Martin et al. 2011). Force data were collected using PCB model 208C01 single-axis piezoelectric force transducers (PCB Piezotronics, Depew, NY). The signals from the transducers were sent to individual PCB 484B11 signal conditioners – one conditioner per sensor – and then digitized at 1  $kHz$  using a 16-bit National Instruments PCI-6052E analog-to-digital card (National Instruments Corp., Austin, TX). Each sensor was mounted on a Linmot PS01-23x80 linear actuator (Linmot, Spreitenbach, Switzerland). Each actuator could be moved independently of the others by means of a Linmot E400-AT four-channel servo drive. Data collection, visual feedback to the subject, and actuator control were all managed using a single program running in a National Instruments LabView environment. Visual feedback was provided by means of a 19" monitor placed 0.8  $m$  from the subject. The feedback cursor (a white dot) showed on the monitor represented total finger force along the vertical axis and total moment of force in a frontal plane computed with respect to a horizontal axis passing through the midpoint between the  $M$  and  $R$  fingers along the horizontal axis. Pronation efforts led to leftward deviation of the feedback cursor. An initial target was placed on the screen (a white circle) corresponding to the total force of 10  $N$  and zero total moment.

The experiment involved two parts: Voluntary force-pulse production and reacting to unexpected perturbations (see later). Prior to each trial, the subjects were asked to place the fingers on the centers of the sensors and relax; sensor readings were set to zero during this time interval. As a result, the sensors measured only active pressing forces. Then, a verbal command was given to the subject and data acquisition started. The subject was given 2  $s$  to place the cursor over the initial target. During the force-pulse trials, the subjects were asked to produce a force pulse from the initial target in less than 1  $s$  by an instructed finger (Figure 9A). Each finger performed three pulse trials in a random order. In perturbation trials, one of the sensors unexpectedly moved up by 1  $cm$  over 0.5  $s$ . This led to an increase in total force (Figure 9B), while changes in the moment of force depended on what finger was perturbed. The subject was instructed to return to the target position as quickly as possible. Each finger was perturbed once per trial, with 10 –  $s$  rest periods between each of the three repetitions. Perturbation conditions were block-randomized between fingers with 1-min rest periods between blocks.

From the pulse trials we manually identified the onsets of the force decrease phase (see Figure 9A). From the perturbation trials we manually identified the on-

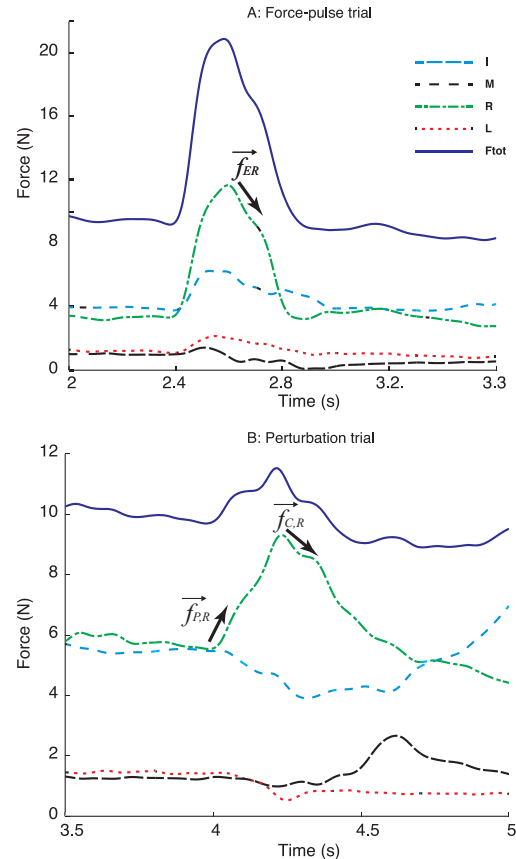


**Fig. 9** Typical time profiles of the force-pulse trial (A, top panel) and perturbation trial (B, bottom panel) performed by a representative subject. The total force profile is shown with the solid trace, and individual finger forces are shown with different dashed traces. The intervals used to compute the eigenvectors in the force space are shown with the arrows.

sets of two time intervals: one corresponding to the perturbation-induced force change and the other corresponding to the earliest corrective action by the subjects. Each time interval contained 200  $ms$  of the four-dimensional finger force ( $I$ ,  $M$ ,  $L$ , and  $R$ ) data. Further, for each time interval, principal component analysis (PCA) based on the co-variation matrix was used to compute the first eigenvector in the four-dimensional finger force space, accounting for most variance across the time samples, for each subject and each trial separately.

Therefore, for each perturbation trial we obtained two eigenvectors in the finger force space. We will refer to these vectors as  $\vec{f}_{P,i}$  (force vector during the perturbation applied to the  $i$ -th finger), and  $\vec{f}_{C,i}$  (force vector during the earliest correction in trials with perturbations applied to the  $i$ -th finger). For each finger, from the three force-pulses trials we computed an average vector  $\vec{f}_{E,i}$  (force vector during the downward phase of force change in the pulse task by the  $i$ -th fin-

ger). Note that this vector reflected the unintentional force production by non-task fingers of the hand (enslaving).

Finally, we computed the angles  $\alpha_{PE}$  (averaged across repetitions) between  $\vec{f}_{P,i}$  and  $\vec{f}_{E,i}$  and angles  $\alpha_{PC}$  between  $\vec{f}_{P,i}$  and  $\vec{f}_{C,i}$  for each finger and each subject separately. The Harrison-Kanji test, which is an analog of two-factor ANOVA for circular data, was used with FINGER (4 levels:  $I, M, R, L$ ) and ANGLE (2 levels,  $\alpha_{PE}$  and  $\alpha_{PC}$ ) as factors. All data analysis were performed in Matlab (MathWorks, Inc.) software.

### 3.2.2 The results - acting along the most nimble direction

During the force-pulse trials, forces of all four fingers changed in parallel (Figure 9A). There was a larger change in the force produced by the instructed finger and smaller changes in the other finger forces. These patterns are typical of enslaving reported in earlier studies [44, 6]. PCA applied to the finger force changes produced similar results over the phase of force increase and the phase of force drop. The first PC accounted for over 95% of the total variance in the finger force space in all subjects and for each finger as the instructed finger. The loading factors at individual finger forces were of the same sign.

In the perturbation conditions, lifting a finger’s force sensor produced a complex pattern of changes in the forces produced by all four fingers (similar to the results described in [21, 40]). Typically, the force of the perturbed finger increased, while the forces produced by the three other fingers dropped (Figure 9B). The total force increased. The first PC accounted for over 95% of the total variance in the finger force space in all subjects and for each finger as the perturbed finger. The loading factors at different fingers were of different signs; most commonly, the perturbed finger loading was of a different sign as compared to the loading of the three other fingers.

Overall, the angle between the vectors of perturbation and correction ( $\alpha_{PC}$ ) was consistently lower than the one between the vectors of perturbation and voluntary force drop ( $\alpha_{PE}$ ). These results are illustrated in Figure 10, which shows averaged (across subjects) values of the two angles with standard error bars. The gross average of  $\alpha_{PC}$  was  $15.9 \pm 6.6^\circ$ , while it was  $25.9 \pm 10.9^\circ$  for  $\alpha_{PE}$ . The Harrison-Kanji test confirmed the main effect of angle ( $F_{[1,56]} = 19.17, p < 0.0001$ ) without other effects.

Overall, these results confirm one of the predictions of the AMN-rule. Indeed, the first reactions to perturbations in the four-dimensional finger force space

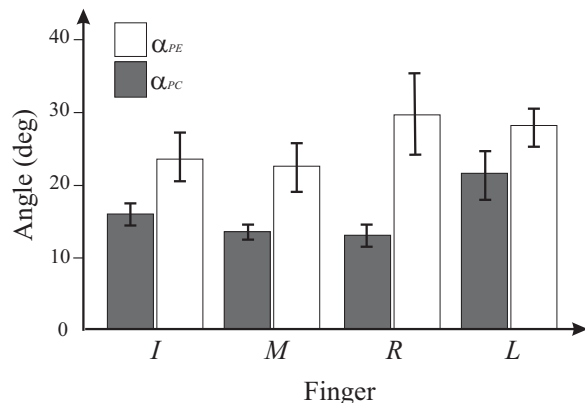


**Fig. 10** The angles between the force vector produced by a quick perturbation applied to a finger and the force vector during the downward phase of the force-pulse trial by the same finger ( $\alpha_{PE}$ ) and between the first vector and the vector of the corrective action ( $\alpha_{PC}$ ). Averaged across subjects data are shown with standard error bars. Note that for each finger as the target finger  $\alpha_{PE} < \alpha_{PC}$ .

showed relatively small angles with the vector reflecting the effects of the perturbation on finger forces. This angle was significantly smaller as compared to typical subject-specific finger force vectors produced when the subjects tried to increase or decrease force with one finger (the perturbed finger) only.

## 4 Discussion: The Stability Search Algorithm Hypotheses within the Context of Motor Control Hypotheses

The most important axiom forming the foundation of our approach is that we assume the existence of task-specific coordinate systems organized to allow effective local control. A particular implementation of local control has been addressed as the “act on the most nimble” (AMN) rule. We have shown that this method can solve problems better than control with random matrices but loses efficacy with an increase in the task dimensionality, not so much with the system dimensionality. This problem can be overcome by using feedback with adjustable gain, but in this case the system slows down dramatically.

Further, we considered a number of additional rules that improve the outcome. One of them is: If local control does not work, change the coordinate system. More specific rules that all improve probability of reaching stability include the following. Deal with one dimension at a time and do not return back to any of the previously involved dimensions. Organize elemental variables into generations (groups assembled by links to a specific task variable,  $y$ ) by their nimbleness. Allowing bi-local

control improves the performance even more. Bi-local control is an example of implementing the general rule of minimizing non-local actions.

#### 4.1 Systems of Coordinates in Motor Control

One of the important features of the suggested scheme is the identification of three systems of coordinates that can be used to describe processes associated with the neural control of a movement. Most commonly, movement studies operate with variables directly measured by the available systems, for example those that measure kinematic, kinetic, or electromyographic variables. Some of these variables describe overall performance, for example fingertip coordinates during pointing. Other variables reflect processes in elements that contribute to the task-related performance (e.g., joint rotations, digit forces and moments, muscle activation, etc.). Some variables may not be directly measured but computed based on other variables and known (or assumed) parameters of the system (for example, joint torques and muscle forces).

Using measured sets of variables to infer coordinate systems used for the neural control of movement has been a challenge. One of the dominant ideas originating from the classical studies by Bernstein [5] has been that elements are united by the central nervous system into relatively stable groups to reduce the number of parameters manipulated at task-related neural levels. Such groups have been addressed as “synergies” [8, 38] or “modes” [42, 14]. Here, we are going to address such groups as “modes” to avoid confusion with another definition of synergies as neural structures that ensure stability of performance based on modes (reviewed in [15]). Some studies emphasized the relative invariance of the mode composition across tasks [12, 39, 38] while other studies showed that the modes could be rearranged quickly with changes in the stability requirements [14, 7]. We believe that some of the disagreements may originate from using the same term for different coordinate systems.

Within our scheme, measured variables produced by elements (e.g., digit forces, joint rotations, and muscle activations) are united into modes that are relatively stable across task variations. These modes may reflect preferred changes in the referent body configuration (cf.[10]) based on the person’s experience with everyday tasks. Mode composition is reflected in the structure of response to a noisy external input and can be reconstructed using matrix factorization techniques such as principal component analysis, factor analysis, independent component analysis, and non-negative ma-

trix factorization (reviewed in [37]). Unlike many earlier studies, we do not assume that the number of modes (the dimensionality of the space where the control process takes place,  $x_i$  in our notation) is smaller than the number of measured variables. It may be larger. For example, in our experiment, forces of four fingers were measured. The dimensionality of  $x_i$  may be higher corresponding, for example, to the number of muscles or muscle compartments involved in the task.

According to our main assumption, there is another coordinate system that allows ensuring stability of performance using local control organized about each axis. We suggest using a term “control coordinates” for this system. Unlike modes, control coordinates are sensitive to task changes, particularly to changes in conditions that affect stability of performance. When a person encounters a novel task, however, he/she searches for an adequate set of control coordinates that would allow implementing local control rules.

Our experiment showed that a quick reaction to unexpected perturbations acts along directions in the finger force space that are close to the directions of finger force deviations produced by the perturbations. In contrast, these reactions formed larger angles with vectors reflecting finger modes [6], eigenvectors in the space of finger forces that reflect finger force changes when a person tries to act with one finger at a time. This result corroborates the idea that a quick corrective actions are organized not along mode directions but along axes of another coordinate system, close to the ones along which the system shows the quickest deviation in response to the perturbation.

#### 4.2 Relations to the Uncontrolled Manifold and Referent Configuration Hypothesis

Figure 4 offers a block diagram related to the control of the hand based on a few levels. At the upper level, the task is shared between the actions of the thumb and the opposing fingers represented as a single digit (virtual finger, Arbib et al. 1985) with the same mechanical effect as the four fingers combined. Further, the virtual finger action is shared among the actual fingers (our experiments analyze four-finger coordination at that level). Even further, action of a finger is shared among a redundant set of muscles contributing to finger’s action. And at the bottom level, each muscle is organized into a set of motor units by the tonic stretch reflex feedback that stabilizes the equilibrium point of the system “muscle + reflexes + external load”. Only the last level may be seen as based on relatively well-

known neurophysiological mechanisms with the threshold of the tonic stretch reflex ( $\lambda$ ) serving as a control (input) variable for the muscle [9].

In more intuitive terms, consider controlling the motion of a donkey using a carrot. The carrot trajectory defines time evolution of referent coordinates for the head trajectory, to which the head is attracted. But the head cannot move without moving the legs. So, this big carrot is translated into a redundant set of smaller mini-carrots for individual legs; and then, into even more micro-carrots for the joints and muscles. Coordinates of such carrots for salient body parts represent referent body configuration.

While the scheme in Figure 4 ensures some stability properties of the action, changes in the overall organization of action (e.g., changes in the RC trajectories) may be needed if the task changes or there is a major change in the external force field. The general principles suggested in this paper offer a solution for the problem of stabilizing action in such conditions.

A few recent studies have shown that, when a major change in the external conditions of task execution takes place, corrective actions are seen in both range (ORT) and self-motion (UCM) spaces with respect to task-specific performance variables [23,24]. Moreover, self-motion dominates, which, by definition, is unable to correct the action. These observations suggest that no single economy principle can form the foundation for such corrections. They allow interpretation within the set of principles suggested in this paper. Any perturbation is expected to induce large effects in less stable directions (those that span the UCM) as compared to more stable directions (ORT). According to the AMN-rule, corrective action is organized along the most nimble of the coordinates that allow local control. Since the projection of the “most nimble” coordinate to the UCM is expected to dominate, one can expect the corrective action to be primarily directed along the UCM as well.

### 4.3 Reasonably Sloppy Control May be Good Enough

Several recent publications presented arguments in favor of the general idea that the CNS may not solve typical problems perfectly but rather use a set of simple rules that lead to acceptable solutions for most problems [15,20]. Sometimes, the rules fail to solve specific problems and then healthy people make mistakes, fall, mishandle objects, spill coffee, etc. We presented a particular instantiation of such a set of rules (based on the AMN-rule) and showed that these rules were able to stabilize action with high probability. The experimental demonstration of relatively small angles between the

vectors of perturbation-induced force changes and corrective changes in finger forces support the feasibility of the AMN-rule.

Experimental studies of the effects of practice on stability of redundant systems have shown the existence of two stages (reviewed in [15]). First, when a person learns a new task, stability in relevant directions is developed reflected in an increase in the relative amount of variance along directions that span the UCM for the salient performance variables. Then, when accuracy of performance reaches a certain ceiling, further practice leads to a drop of variance in those seemingly irrelevant directions. Why would a person stabilize directions that have no clear effect on overall task performance? We addressed this issue in the section on perfectionism.

Selection of a particular point (range) within the solution space has been discussed as resulting from optimizing the action with respect to some objective (cost) function [25]. Note that only one point on the solution hyper-surface is optimal with respect to any given cost function. Other points within the UCM violate the optimality principle even though they lead to seemingly perfect performance. In a sense, large variance within the UCM combined with low variance orthogonal to the UCM implies that the person is accurate but sloppy. In the course of practice, when the person is as accurate as one can possibly be with respect to the explicit task, further practice may stabilize directions within the UCM to ensure that performance remains as close as possible to optimal with respect to a selected criterion. This is what we call “perfectionism”. Note that perfectionism is never absolute (“nobody is perfect”), and the system remains sloppy, but the degree of sloppiness can be reduced.

We are grateful to Yen-Hsun Wu and Sasha Reschetchko for their help with the experiments.

## References

1. Akulin VM, (2014) Dynamics of Complex Quantum Systems, Second Edition, Springer Dordrecht Heidelberg, New York, London, pp. 195-260..
2. Arbib MA, Iberall T, Lyons D (1985) Coordinated control programs for movements of the hand. In: Goodwin AW and Darian-Smith I, eds. Hand Function and the Neocortex. Berlin: Springer Verlag; pp. 111-129.
3. Asaka T, Wang Y, Fukushima J, Latash ML (2008) Learning effects on muscle modes and multi-mode synergies. *Experimental Brain Research* 184: 323-338.
4. Bernstein NA (1930) A new method of mirror cyclographie and its application towards the study of labor movements during work on a workbench. *Hygiene, Safety and Pathology of Labor*, # 5, p. 3-9, and # 6, p. 3-11. (in Russian).
5. Bernstein NA (1967) The Co-ordination and Regulation of Movements. Pergamon Press, Oxford

6. Danion F, Schöner G, Latash ML, Li S, Scholz JP, Zatsiorsky VM (2003) A force mode hypothesis for finger interaction during multi-finger force production tasks. *Biological Cybernetics* 88: 91-98.
7. Danna-Dos-Santos A, Slomka K, Zatsiorsky VM, Latash ML (2007) Muscle modes and synergies during voluntary body sway. *Experimental Brain Research* 179: 533-550.
8. d'Avella A, Saltiel P, Bizzi E (2003) Combinations of muscle synergies in the construction of a natural motor behavior. *Nature Neuroscience* 6: 300-308.
9. Feldman AG (1986) Once more on the equilibrium-point hypothesis ( $\lambda$ -model) for motor control. *Journal of Motor Behavior* 18: 17-54.
10. Feldman AG (2009) Origin and advances of the equilibrium-point hypothesis. *Advances in Experimental Medicine and Biology* 629: 637-643.
11. Gelfand IM, Latash ML (1998) On the problem of adequate language in movement science. *Motor Control* 2: 306-313.
12. Ivanenko YP, Cappellini G, Dominici N, Poppele RE, Lacquaniti F (2005) Coordination of locomotion with voluntary movements in humans. *Journal of Neuroscience* 25: 7238-7253.
13. Kilbreath SL, Gandevia SC (1994) Limited independent flexion of the thumb and fingers in human subjects. *Journal of Physiology* 479: 487-497.
14. Krishnamoorthy V, Goodman SR, Latash ML, Zatsiorsky VM (2003) Muscle synergies during shifts of the center of pressure by standing persons: Identification of muscle modes. *Biological Cybernetics* 89: 152-161.
15. Latash ML (2008) *Synergy*. Oxford University Press: New York.
16. Latash ML (2010) Motor synergies and the equilibrium-point hypothesis. *Motor Control* 14: 294-322.
17. Latash ML (2012) The bliss (not the problem) of motor abundance (not redundancy). *Experimental Brain Research* 217: 1-5.
18. Latash ML, Scholz JP, Schöner G (2007) Toward a new theory of motor synergies. *Motor Control* 11: 276-308.
19. Li ZM, Latash ML, Zatsiorsky VM (1998) Force sharing among fingers as a model of the redundancy problem. *Experimental Brain Research* 119:276-286
20. Loeb GE (2012) Optimal isn't good enough. *Biological Cybernetics* 106: 757-765.
21. Martin JR, Budgeon MK, Zatsiorsky VM, Latash ML (2011) Stabilization of the total force in multi-finger pressing tasks studied with the 'inverse piano' technique. *Human Movement Science* 30: 446-458.
22. Martin V, Scholz JP, Schöner G (2009) Redundancy, self-motion, and motor control. *Neural Computing* 21, 1371-1414.
23. Mattos D, Latash ML, Park E, Kuhl J, Scholz JP (2011) Unpredictable elbow joint perturbation during reaching results in multijoint motor equivalence. *Journal of Neurophysiology* 106: 1424-1436.
24. Mattos D, Kuhl J, Scholz JP, Latash ML (2013) Motor equivalence (ME) during reaching: Is ME observable at the muscle level? *Motor Control* 17:145-175.
25. Prilutsky BI, Zatsiorsky VM (2002) Optimization-based models of muscle coordination. *Exercise and Sport Science Reviews* 30: 32-38
26. Schieber MH, Santello M (2004) Hand function: peripheral and central constraints on performance. *Journal of Applied Physiology* 96: 2293-300.
27. Scholz JP, Schöner G (1999). The uncontrolled manifold concept: Identifying control variables for a functional task. *Experimental Brain Research* 126, 289-306.
28. Schöner G (1995) Recent developments and problems in human movement science and their conceptual implications. *Ecological Psychology* 8: 291-314.
29. Simon Models of bounded rationality. MIT Press; Cambridge, MA: 1982. Ben-Haim Y. Info-gap Decision Theory: Decisions under severe uncertainty. Academic Press; London: 2006.
30. Georgopoulos AP, Kalaska JF, Caminiti R, Massey JT (1982) On the relations between the direction of two-dimensional arm movements and cell discharge in primate motor cortex. *Journal of Neuroscience* 2: 1527-1537.
31. Georgopoulos AP, Schwartz AB, Kettner RE (1986) Neural population coding of movement direction. *Science* 233: 1416-1419.
32. Schwartz AB, Moran DW (2000) Arm trajectory and representation of movement processing in motor cortical activity. *Eur J Neurosci.* 12(6):1851-6.
33. Amirikian B, Georgopoulos AP (2003) Motor cortex: Coding and decoding of directional operations. In: Arbib MA (Ed.) *The Handbook of Brain Theory and Neural Networks*, Second Edition, pp. 690-701, MIT Press: Cambridge, MA.
34. Slobounov S, Chiang H, Johnston J, Ray W (2002) Modulated cortical control of individual fingers in experienced musicians: an EEG study. *Electroencephalographic study.* *Clinical Neurophysiology* 113: 2013-2024.
35. Stein RB, Gossen ER, Jones KE (2005) Neuronal variability: noise or part of the signal? *Nature Reviews in Neuroscience* 6(5): 389-97.
36. Terekhov AV, Pesin YB, Niu X, Latash ML, Zatsiorsky VM (2010) An analytical approach to the problem of inverse optimization: An application to human prehension. *Journal of Mathematical Biology* 61: 423-453.
37. Ting LH, Chvatal SA (2010) Decomposing muscle activity in motor tasks: Methods and Interpretation. In: Danion F, Latash ML (Eds) *Motor Control: Theories, Experiments, and Applications*, p. 102-139, Oxford University Press: New York, NY.
38. Ting LH, Macpherson JM (2005) A limited set of muscle synergies for force control during a postural task. *Journal of Neurophysiology* 93: 609-613.
39. Torres-Oviedo G, Ting LH (2007) Muscle synergies characterizing human postural responses. *Journal of Neurophysiology* 98: 2144-2156
40. Wilhelm L., Zatsiorsky V.M., Latash M.L. (2013) Equifinality and its violations in a redundant system: Multi-finger accurate force production. *Journal of Neurophysiology* 110: 1965-1973.
41. Wu YH, Pazin N, Zatsiorsky VM, Latash ML (2013) Improving finger coordination in young and elderly persons. *Experimental Brain Research* 226: 273-283.
42. Zatsiorsky VM, Li ZM, Latash ML (1998) Coordinated force production in multi-finger tasks: Finger interaction and neural network modeling. *Biological Cybernetics* 79: 139-150.
43. Zatsiorsky VM, Duarte M (1999) Instant equilibrium point and its migration in standing tasks: rambling and trembling components of the stabilogram. *Motor Control.* 3(1):28-38.
44. Zatsiorsky VM, Li ZM, Latash ML (2000). Enslaving effects in multi-finger force production. *Experimental Brain Research* 131: 187-195.